CHARACTERIZING SEISMICITY AND ITS GEOLOGICAL ASSOCIATION IN NORTHEASTERN NORTH AMERICA WITH RELATIVE LOCATION AND EMPIRICAL GREEN'S FUNCTIONS

Contract no. 1434-94-G-2421

M. Nafi Toksöz
Massachusetts Institute of Technology
Earth Resources Laboratory
42 Carleton Street
Cambridge, Massachusetts 02142
(617)-253-7852
FAX: (617)-253-6385
email: nafi@erl.mit.edu
Program Element II.2

Research supported by the U.S. Geological Survey (USGS), Department of the Interior, under USGS award number 1434-94-G-2421. The views and conclusions contained in this document are those of the authors and should not be interpreted as necessarily representing the official policies, either expressed or implied, of the U.S. Government.

TABLE OF CONTENTS

CHAPTER 1

SOURCE CHARACTERIZATION AND FAULT PLANE DETERMINATIONS FOR M_{bLg} = 1.2 TO 4.4 EARTHQUAKES IN THE CHARLEVOIX SEISMIC ZONE, QUEBEC, CANADA

YINGPING LI, CHARLES DOLL, JR., AND M. N. TOKSÖZ

Earth Resources Laboratory

Department of Earth, Atmospheric, and Planetary Sciences

Massachusetts Institute of Technology

Cambridge, MA 02139

Tel: (617)-253-7796

Fax: (617)-253-6385

Submitted to Bulletin of the Seismological Society of America

September 30, 1994

ABSTRACT

Two earthquake multiplets and two doublets recorded by the Charlevoix Telemetered Network (CLTN) in the Charlevoix Seismic Zone (CSZ) of southern Quebec, Canada have been analyzed using an empirical Green's function (EGF) method to derive the relative source time functions (STFs) of seven master events with M=1.2-4.4. We identified the multiplets and doublets by applying a waveform cross-correlation and relative event location technique to verify that a potential earthquake pair satisfied the criteria of having similar focal mechanisms and hypocentral locations. Three-component S waveforms recorded by the high dynamic range (126 dB) instrumentation of the CLTN were used to extract the STFs.

The STFs reveal that six of the seven events are simple with single source pulses having durations of 0.05 to 0.2 s. Another earthquake (920310-0545, M3.3) appears to be a double event with two episodes of rupturing. Azimuthal variations of the pulse amplitudes and widths of the STFs provide strong evidence for the rupture directivities of five of the earthquakes (M=1.2-4.4). These results demonstrate that microearthquakes in the CSZ can have both rupture directivity and a complex rupture process. The azimuthal variations in pulse amplitudes of the STFs were used to estimate the rupture directions and rupture velocities. Estimated rupture velocities range from 0.5 to $0.7V_S$. Estimates of the rupture direction were combined with P wave focal mechanisms for the four largest events (M3.3-4.4) to infer the actual fault plane for these earthquakes. Source parameters were measured for the retrieved STFs of the master events, including seismic moments of 3.5×10^{18} to 5.3×10^{21} dyne-cm, fault radii of 100-330 m, and static stress drops of 2 to 90 bars. The fault radii and stress drop estimates for $M > 3$ events agree well with estimates obtained by other researchers for $M \sim 3$ to 4.5 earthquakes in the CSZ (Boatwright, 1994; Atkinson and Somerville, 1994). We also observed apparent scaling between the stress drop and the earthquake size, which has been reported in other studies of stress drop in northeastern North America.(*e.g.*, Boatwright, 1994; Shi *et al.*, 1994).

INTRODUCTION

The source time function (STF) of an earthquake contains important parameters that characterize the rupture process and source properties of the earthquake. However, the extraction of the STF from observed seismograms requires isolating the source effects from those of the path, site, and instrument response. One approach to remove the effects of the path, site, and instrument response from observed seismograms is to use the empirical Green's function (EGF) deconvolution method (*e.g.*, Mueller, 1985; Frankel *et al.*, 1986; Li and Thurber, 1988). The advantage of this method is that detailed knowledge of the earth structure, instrument response and attenuation effects is not required. For two earthquakes having similar hypocenters and focal mechanisms, but different sizes, one can treat the waveform of the smaller event as the EGF (Hartzell, 1978) and deconvolve it from that of the larger event to obtain a relative STF for the larger earthquake (Mueller, 1985). Since the pair of events is recorded at the same station by the same instrument and shares the same propagation path, the deconvolution method should result in an STF which is corrected for the path, site, and instrument effects.

The EGF deconvolution method has been successfully applied to extract STFs for microearthquakes in California (Frankel *et al.*, 1986; Hutchings and Wu, 1990; Mori and Frankel, 1990; Mori and Hartzell, 1990; Hough *et al.*, 1991; Mori, 1993), Hawaii (Li and Thurber, 1988), New York (Xie *et al.*, 1991), Miramichi, Canada (Mueller, 1985), and Yunan, China (Chen *et al.*, 1991), using waveform data recorded by local seismic networks. The retrieved STFs have been used to estimate the source parameters, such as rising time, source duration, seismic moment ratio, fault radius, and stress drop (*e.g.*, Frankel *et al.*, 1986; Li and Thurber, 1988; Mori and Frankel, 1990; Xie *et al.*, 1991). Analysis of the STFs also has revealed the rupture complexity and rupture directivity of microearthquakes (*e.g.*, Frankel *et al.*, 1986; Li and Thurber, 1988; Mori and Frankel, 1990). It has been demonstrated that the rupture directivity along with the focal mechanism of an earthquake can be used to determine which of the two nodal planes is the actual fault plane (Frankel *et al.*, 1986; Li and Thurber, 1988; Mori and Hartzell, 1990; Mori, 1993).

The objective of this study is to examine the rupture directivity and complexity and to estimate source parameters of microearthquakes in the Charlevoix Seismic Zone (CSZ), Quebec, Canada (Figure 1). Although spectral analysis techniques have been used to estimate the source parameters for M=3-5 earthquakes in the CSZ (*e.g.*, Hasegawa and Wetmiller, 1980; Boatwright, 1994; Atkinson and Somerville, 1994), the EGF method has not been applied to extract the STFs and estimate the source parameters for earthquakes in this seismic source zone. In this paper, we used the EGF method to retrieve the relative STFs and to analyze the source properties of seven of the larger microearthquakes (M_{bLg} =1.2 to 4.4) from four groups of events located in the CSZ. Three-component S waveforms of smaller events in each group, treated as the EGFs, were deconvolved from those of the larger earthquakes to obtain their STFs. Our results indicate that the STFs of six events are single pulses with source durations of 0.05 to 0.2 s and one earthquake (920310-0545, M_{bLg}=3.3) appears to be a double event. We estimated the source parameters, such as the rupture velocity, fault length, moment release, and stress drop, for these events based on the time domain analysis of the STFs. Azimuthal variation of the pulse amplitudes and widths of the STFs provide strong evidence for the rupture directivities of five of the earthquakes with magnitudes ranging from 1.2 to 4.4. The rupture directivities along with P first motion fault plane solutions of the four largest events ($M_{bLg} \geq 3.3$) permit determination of the rupture planes and characterization of the rupture processes of these earthquakes.

CHARLEVOIX SEISMIC ZONE AND NETWORK DATA

The Charlevoix Seismic Zone (CSZ) is defined as a 80 x 35 km rectangle located along the St. Lawrence River (Figure 1) in southern Quebec and is among the most seismically active areas in

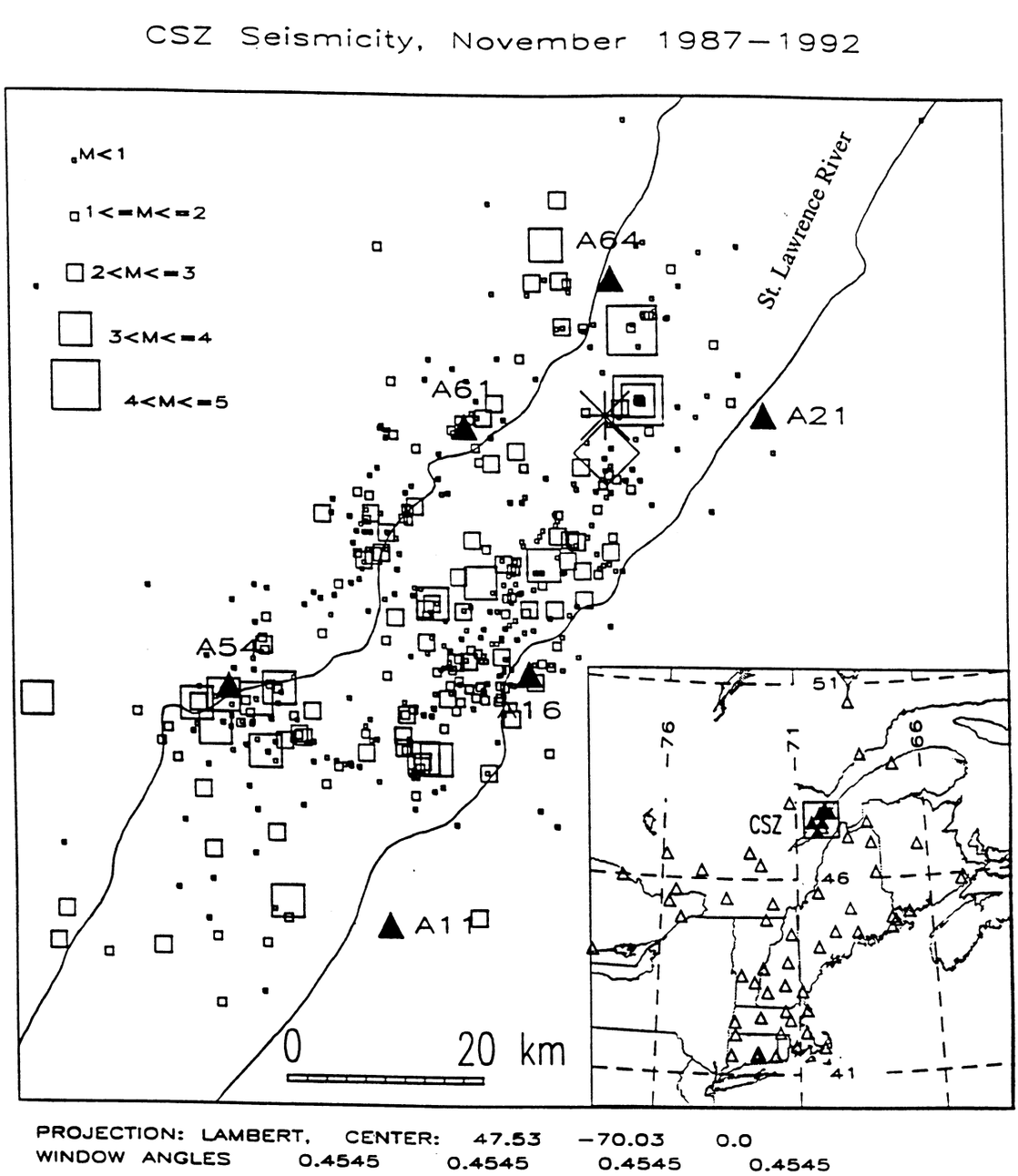

Figure 1. Seismicity (squares) of the Charlevoix Seismic Zone (CSZ) in Quebec, Canada for November 1987-1992. The 1925 (m_b=6.5) and the 1979 (m_b=5.0) earthquakes are shown as an asterisk and a diamond, respectively. The filled triangles mark the locations of the CLTN stations. The inset map depicts the location of the CSZ in northeastern North America and the sites of the ECTN and the NESN stations (open triangles), many of which were used to determine the focal mechanisms of the larger microearthquakes studied.

eastern North America (Buchbinder *et al.*, 1988). Historically, the CSZ has been the location of several large earthquakes (Smith, 1962). The largest instrumentally recorded earthquake of this group occurred on March 1, 1925 with m_b = 6.5 (Stevens, 1980; Ebel *et al.*, 1986; Bent, 1992). Damage to buildings from this earthquake was caused at distances as great as 240 km away (Hodgson, 1950). The latest potentially damaging earthquake (m_b = 5) occurred on August 19, 1979 (Hasegawa and Wetmiller, 1980).

The waveform data used in this study were recorded by the Charlevoix Telemetered Network (CLTN) operated by the Canadian Geological Survey. The CLTN consists of six three-component stations located in groups of three each along the northwest and southeast shorelines of the St. Lawrence River (Figure 1). These stations are situated parallel to the general northeasterly strike and bound the seismicity of the CSZ (Buchbinder *et al.*, 1988). The CLTN is a short-period local network which was modernized in November 1987 to include digital recording at a rate of 80 sps and three-component instruments with automatic gain control to insure a wide dynamic range of 126 dB (Munro, personal communication). The wide dynamic range of the instrument allows recording of seismic waveforms of M0-5 earthquakes on scale at local distances and is especially suitable for the EGF analysis.

On March 9, 1989, an earthquake (M_{bLg} = 4.3) occurred in the upper CSZ and was followed by a larger event (M_{bLg}=4.4) in the same place about 47 hours later. Wetmiller and Adams (1990) identified these two events as a doublet, meaning two earthquakes having a similar hypocentral location and focal mechanism. Since the M_{bLg} 4.3 event was followed by two smaller aftershocks with similar locations, we defined this group of four events as a multiplet. Figure 2 shows three-component seismograms for the four earthquakes of the multiplet recorded at station A61. Waveforms of the four events with magnitudes ranging from 0.2 to 4.4 show a striking similarity, with the maximum amplitude of the largest event exceeding that of the smallest by a factor of about 1000. The waveform similarity suggests that the multiplet has hypocenters very close to each other and very similar focal mechanisms.

Applying the cross-correlation analysis and relative location technique to digital waveform data from the CLTN, we identified more doublets and multiplets in the CSZ. Figure 3 shows the epicentral locations of the eleven earthquakes of the two multiplets and two doublets used in this study. In addition to CLTN data, P first motion data from two regional networks (Figure 1), the Eastern Canada Telemetered Network (ECTN, operated by the Canadian Geological Survey) and the New England Seismic Network (NESN, jointly operated by the Weston Observatory of Boston College and the Earth Resources Laboratory of MIT), were also used to constrain the focal mechanisms (Figure 4) for the four largest earthquakes ($M_{bLg} \geq 3.3$) of the four groups of events in the study. A computer method developed by Guinn and Long (1977) was used to find the fault plane solution (or set of solutions) which yields the best match of calculated and observed P first motions. SH waveforms, resulting from the rotation of the horizontal components recorded by the CLTN stations, were used to place additional constraint on the earthquake focal mechanisms. SH focal mechanisms (Figure 4), generated using the strike, dip and rake of the P focal mechanism solutions for the four largest earthquakes, were found to be completely consistent with the projections of the observed SH first motions on the lower focal hemispheres.

RELATIVE EVENT LOCATIONS AND SIMILAR FOCAL MECHANISMS

The EGF deconvolution method requires that the larger earthquake and the smaller EGF event have a similar hypocenter and focal mechanism, so that the deconvolution procedure can effectively remove the path, site and instrument effects. It has been demonstrated that precise relative locations for a cluster of earthquakes are important, not only for selecting appropriate EGF events,

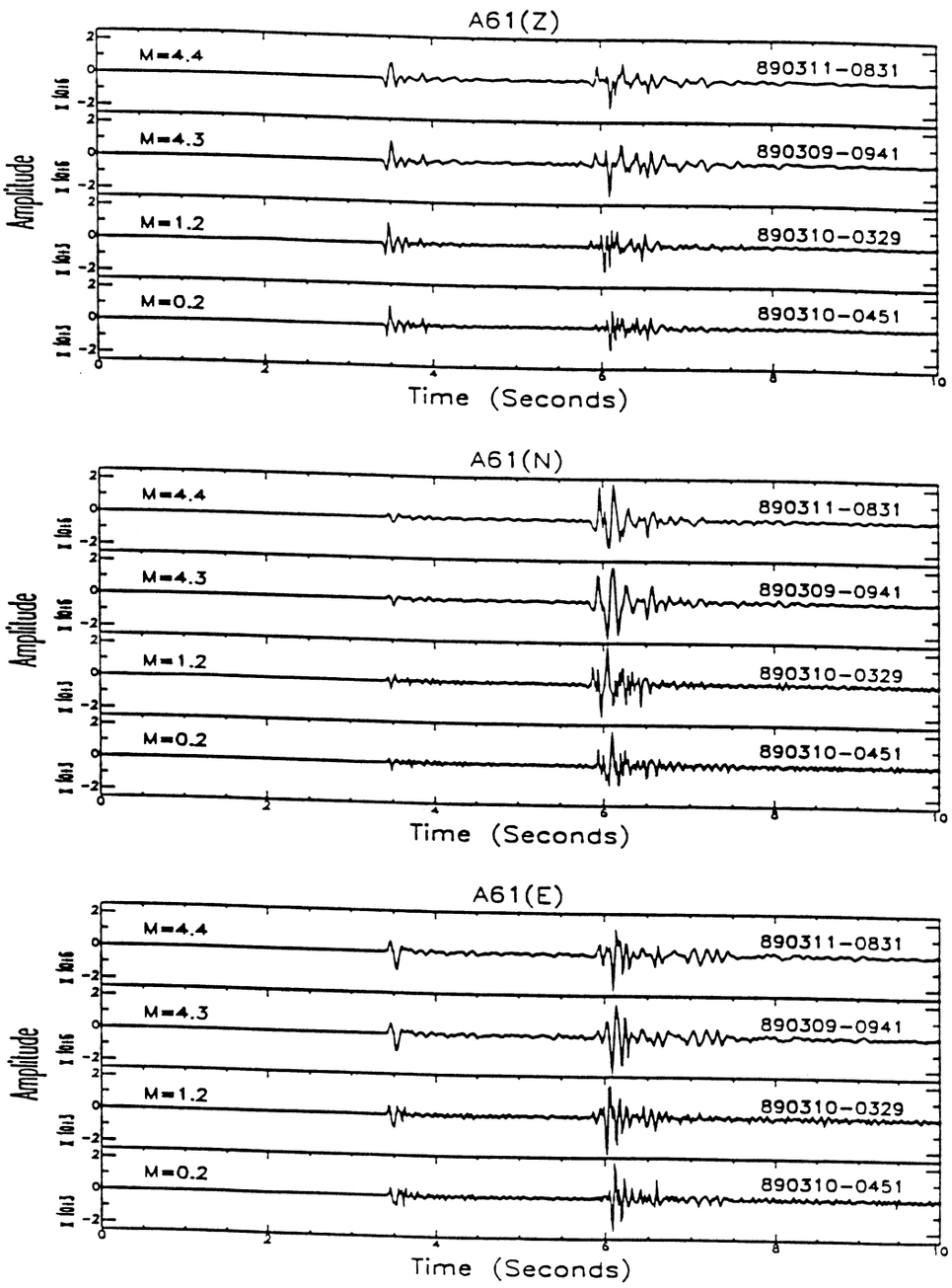

Figure 2. Three-component waveforms of a multiplet of four earthquakes (M=0.2-4.4) recorded at Station A61. The strong similarity of the waveforms is indicative of events which occurred very near one another with similar focal mechanisms. The difference in peak amplitudes between the M4.4 and M0.2 earthquakes is about 1000.

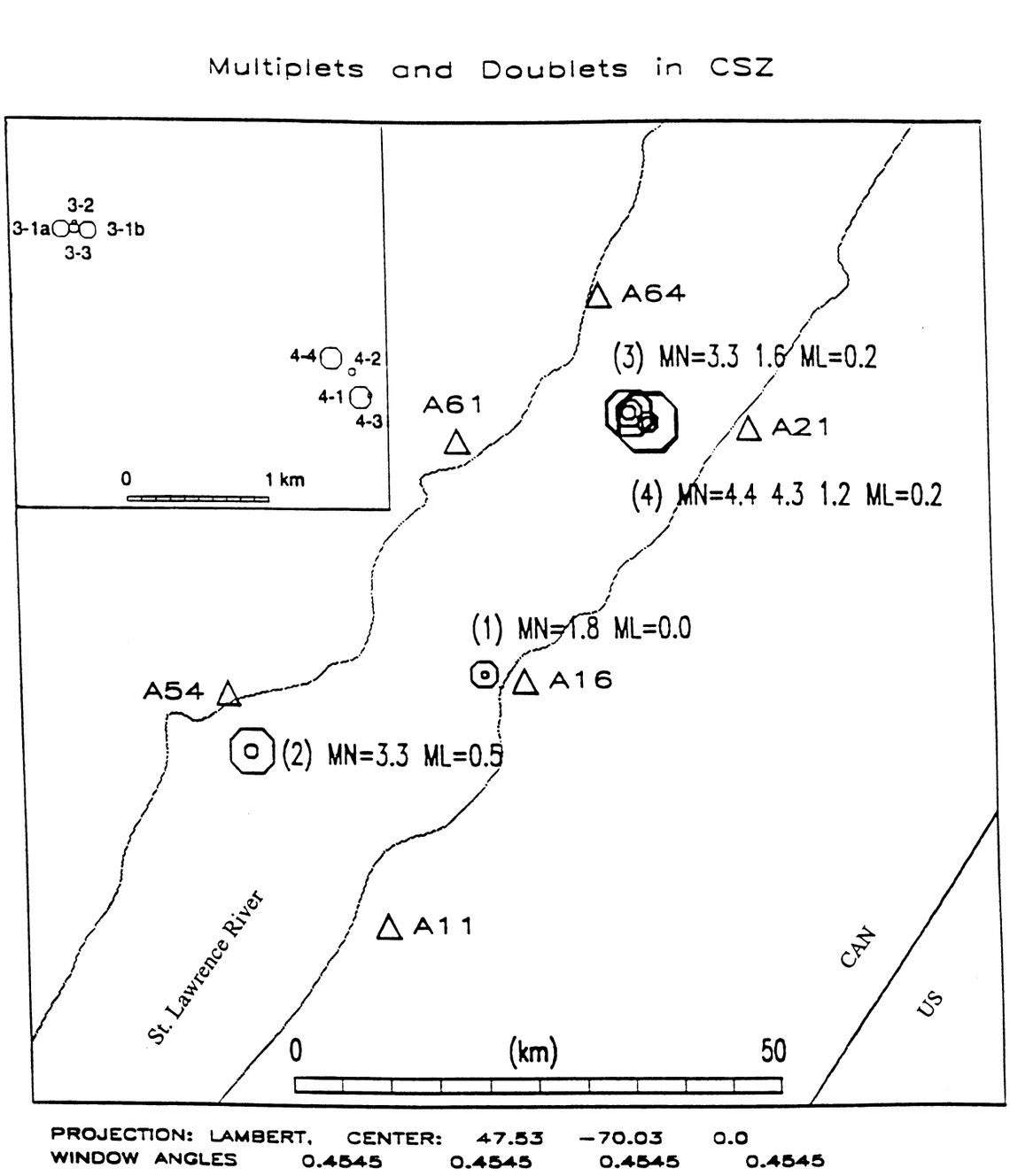

Figure 3. Epicentral locations (octagons) of the two doublets (pairs 1 and 2) and the two multiplets (groups 3 and 4) analyzed in this study. The inset map emphasizes the close spatial separation among the slave and master events of each multiplet resolved by the waveform cross-correlation and relative event location technique.

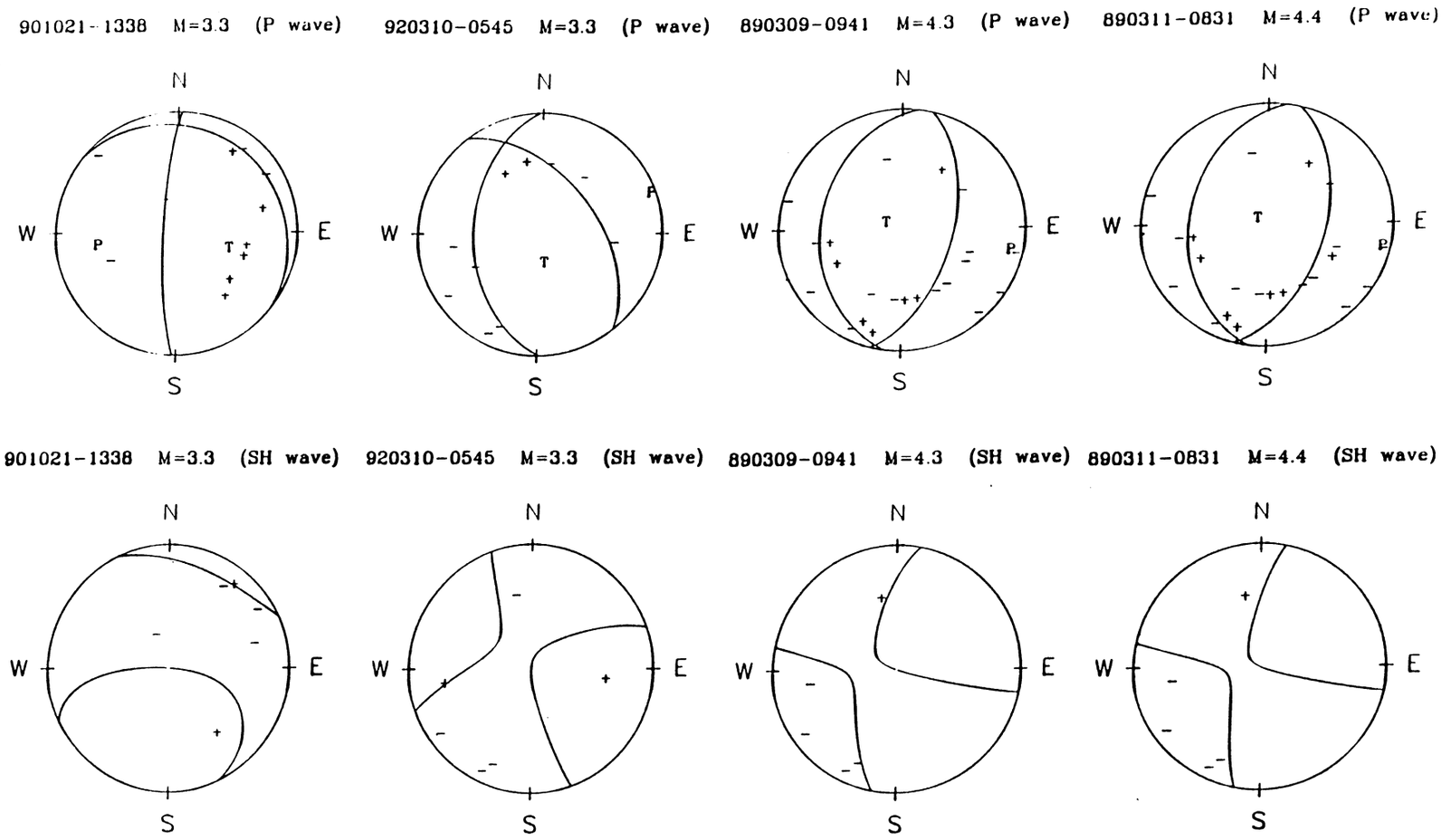

Figure 4. P and SH focal mechanisms for the four largest (M3.3-4.4) earthquakes. P first motion data from the CLTN, ECTN, and NESN were used to constrain the P focal mechanisms. The observed SH polarities fit the SH focal mechanism predicted from the strike, dip and rake of the P focal mechanism for each event.

but also for inferring the rupture directions of larger earthquakes (*e.g.*, Frankel *et al.*, 1986; Mori, 1993).

The principle of the relative event location technique (*e.g.*, Jordan and Sverdrup, 1981; Poupinet *et al.*, 1984; Ito, 1985) is that, for a given seismic phase and receiver, the difference between the arrival times from two events close to one another is much less sensitive to the velocity structure than are the absolute arrival times from each individual event. Therefore, the systematic errors due to an incorrect velocity model will have little effect on the accuracy of the relative event locations.

A cross-correlation analysis technique either in the frequency domain (*e.g.*, Poupinet *et al.*, 1984; Ito, 1985; Fremont and Malone, 1987) or in the time domain (*e.g.*, Frankel, 1982; Pechmann and Kanamori, 1982; Thorbjarnadottir and Pechmann, 1987) has been used to quantitatively characterize the degree of similarity of seismic waveforms from a cluster of earthquakes close in space and to measure their differential arrival times of P and S waves in an accurate, objective, and consistent manner. The conventional time domain analysis typically enables arrival times to be read, at best, to an accuracy of one sample interval, while a cross-spectral analysis can improve the timing precision about an order of magnitude better than the sampling interval. Poupinet *et al.* (1984) and Ito (1985) claimed that, for a waveform with a sampling rate of 100 sps, their method had a timing accuracy of about 1 ms, resulting in a relative location accuracy of 10 m.

We measured the differential arrival time of the P waves on the vertical component seismograms (Figure 5a) from two events near one another using both the cross-correlation and the cross-spectral techniques. Conventional time domain analysis results in a differential arrival time of 0.025 s (Figure 5b), with a timing accuracy of 0.0125 s (instrument sampling rate of 80 sps). The cross-spectral analysis of the P waveforms indicates that the differential arrival time between the two P waves is about 0.021 s (Figure 5c), with a timing resolution of about 1 ms. However, the spectral analysis involves time-consuming calculations and fitting a straight line to the slope of the phase spectrum. We developed a simpler and faster analysis method in the time domain, which gives a timing accuracy similar to the cross-spectral method (Poupinet *et al.*, 1984; Ito, 1985). We oversampled the P wave time series of the master and slave events with an interpolating Finite Impulse Response filter (Tapley and Tull, 1991) and recalculated the cross-correlation function. The maximum peaks of the cross-correlation function are at 0.025 s and 0.020 s for sampling rates of 80 and 200 sps, respectively. Above 400 sps the peaks converge at 0.021 s, which is consistent with the result of the cross-spectral method (Figure 5c).

The cross-correlation function between a master and a slave event was calculated for both P and S wave windows to measure the differential time Δ(S-P) from the time lag between the maximum peaks of correlation coefficients. Figures 6a and 6b show auto-correlation functions of a master event (920314-2128) and cross-correlation functions between the master event and a slave event (920311-0120) for the P and S wave windows. Our modified time domain method also provides the capability to process a double event (Figures 6c and 6d). Cross-correlation functions between the master event and another slave event (920310-0545) for both P and S wave windows show two peaks corresponding to two subevents. At station A61, differential time Δ(S-P) is less than zero for the first subevent and is greater than zero for the second subevent, implying that the first subevent is closer to station A61 and the second one is further away from the station with the master event as a reference. The measurement accuracy of the differential arrival time Δ(S-P) is about 1 ms, resulting in a spatial resolution of about 10 m for the relative hypocenter locations.

We applied the cross-correlation and relative location technique to P and S waveforms recorded by at least four CLTN stations to estimate the relative locations for the eleven earthquakes of the two doublets and two multiplets (Figure 3 and Table 1). In each of the four groups, we selected one earthquake as a master event and calculated its absolute location with S-P times and a one-layer

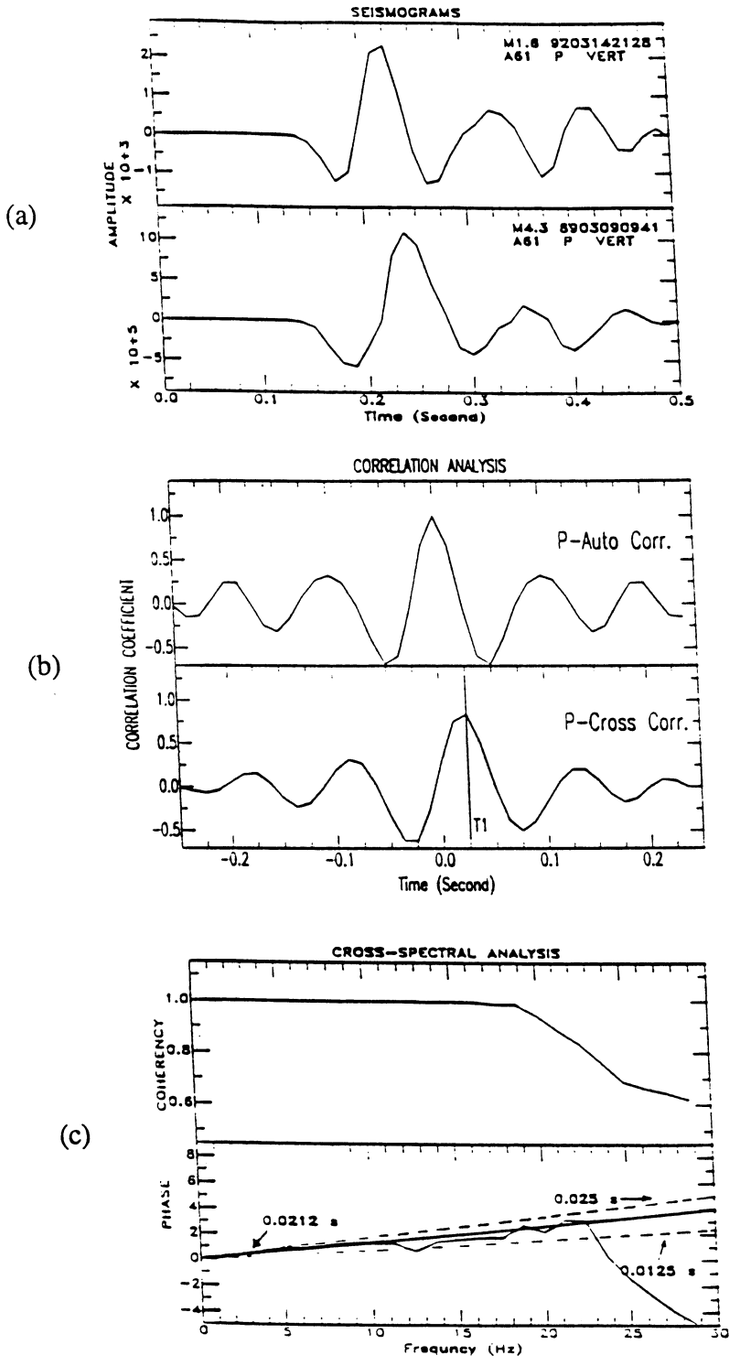

Figure 5. (a) The recorded P waveforms of two earthquakes close in space. (b) The auto-correlation of the first P waveform and cross-correlation of the first with the second P waveform. (c) The coherency and phase spectra of the cross-spectrum of the two P waveforms. The conventional time domain analysis in (b) can only produce a best resolution of one sample interval, resulting in a differential time for P of 0.025s (two samples). The slope (.021 s) best fitted to the phase spectrum in (c) indicates a minimum resolvable time interval of 1 ms by the relationship $2\pi ft$. Oversampling yields an estimate of the P wave differential time of about .021 s, comparable to that of the spectral analysis.

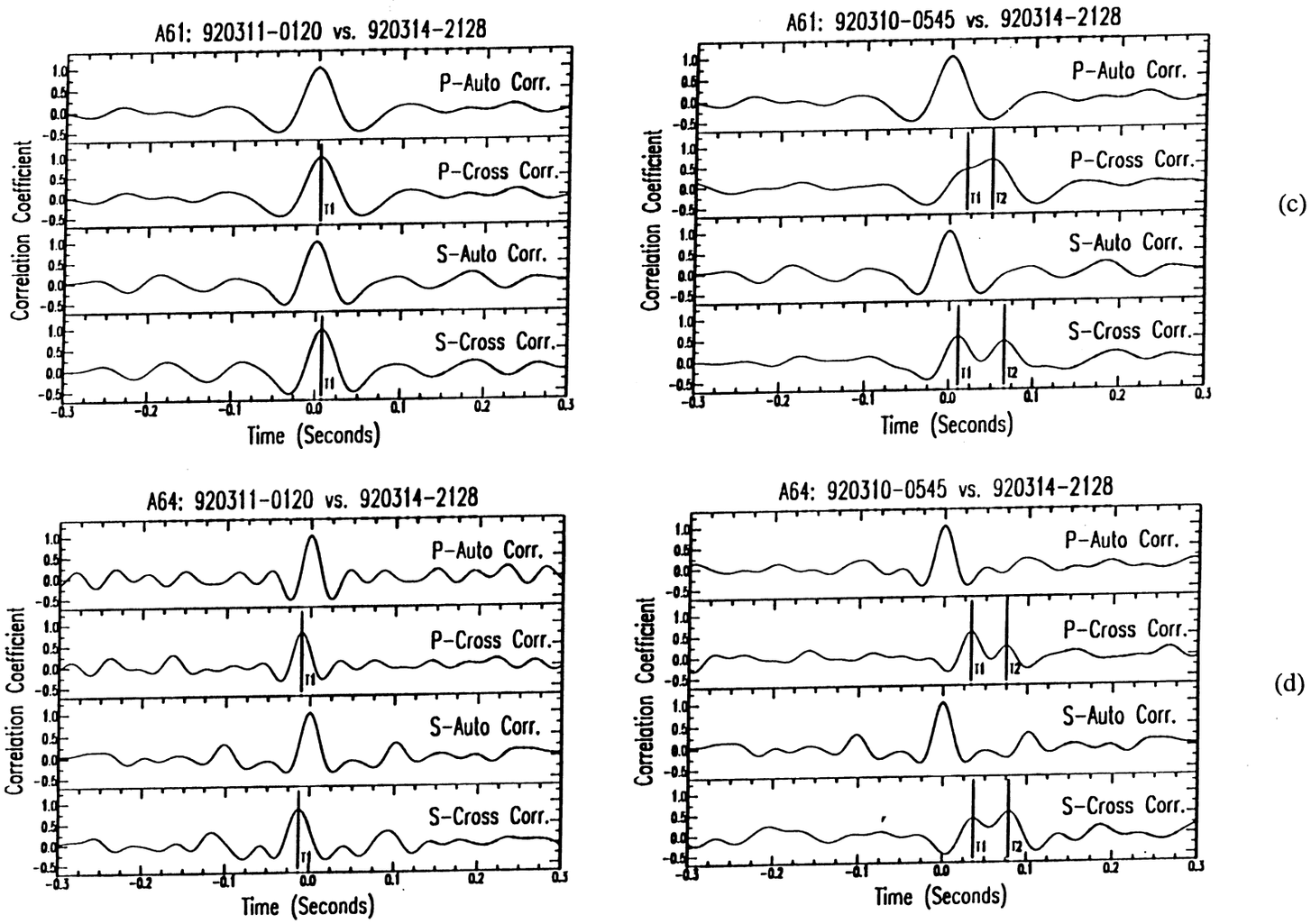

Figure 6. Example of using oversampling with waveform correlation to more accurately measure the differential times of P and S for two event pairs. The time difference (T1) measured for P and S for one event pair (920311-0120 and 920314-2128) is marked on the cross-correlation functions at stations A61 (a) and A64 (b). Event 920310-0545 has two rupture episodes represented by the two high amplitude peaks in the P and S cross-correlation functions at stations A61 (c) and A64 (d). The differential times of P and S between each of the two subevents and the reference event 920314-2128 are marked by T1 and T2, respectively.

Table 1

Hypocentral parameters of earthquakes under study

Group-event No.	Date (YrMoDa)	Time (HrMnSec)	Lat (°)	Lon (°)	Depth (km)	Magnitude* (M_N / M_L)	
1-1	890201	0538 47.5	47.4769	-70.0613	15.03	1.8	
1-2	890915	0216 01.0	47.4765	-70.0605	14.93		0.0
2-1	901021	1338 43.2	47.4032	-70.3803	13.85	3.3	
2-2	901102	0427 50.1	47.4031	-70.3815	13.78		0.5
3-1a†	920310	0545 32.6	47.7181	-69.8556	8.96	3.3	
3-1b†	920310	0545 32.7	47.7180	-69.8531	8.85		
3-2	920311	0120 57.6	47.7184	-69.8544	8.88		0.2
3-3	920314	2128 43.6	47.7181	-69.8544	8.90	1.6	
4-1	890309	0941 32.2	47.7080	-69.8282	8.07	4.3	
4-2	890310	0329 59.5	47.7095	-69.8289	7.98	1.2	
4-3	890310	0451 01.1	47.7081	-69.8273	7.87		0.2
4-4	890311	0831 51.8	47.7103	-69.8308	8.22	4.4	

† A double event.

* The magnitudes were determined by the Canadian Geological Survey. M_L is used for the smallest events recorded only by the CLTN, while M_{bLg} (M_N) is used for the larger events recorded by both the CLTN and the ECTN. On average the M_L scale yields magnitude values 0.4 units less than the M_{bLg} scale for microearthquakes in northeastern North America (Ebel, 1982).

crustal model for the CSZ having an average P wave velocity of 6.2 km/s and a Vp/Vs ratio of 1.73 (Anglin, 1984). Then the differential arrival times Δ(S-P) measured by cross-correlation were used to determine the relative locations of the slave events with respect to the master in each group. The simplified velocity model and different station configurations used for locating master events of different groups may slightly bias absolute locations for the master events about 1 to 2 km, but should have less effect on the relative locations of events in individual groups.

As discussed in a previous section, we have determined the focal mechanisms for the four largest earthquakes among the eleven events. However, insufficient data was available to constrain the focal mechanisms for the smaller events. To insure the larger earthquakes and the EGF events in each group had similar focal mechanisms, we checked the P and SH polarities for the eleven earthquakes with the CLTN data only, and found the P and SH polarities for events in the same group were the same with only one exception (Table 2). At station A21, which is projected close to one of the P wave nodal planes, the P wave polarity of the 920310 event differs from those of the two small aftershocks, reflecting slight differences in the focal mechanisms of the mainshock and aftershocks.

EGF Deconvolution Procedure

Figure 7 illustrates the EGF deconvolution procedure which we used to extract the relative STFs for larger events of the doublets and multiplets. Figure 7 shows tangential S waveforms recorded at station A61 for the three events in one multiplet (M3.3, M1.6 and M0.2) with spatial separations of less than 250 m (Figure 3 and Table 1) and a similar focal mechanism (Figure 4 and Table 2). The seismogram of the smallest event was used as the EGF and deconvolved from those of the two larger events to obtain the STFs for the larger earthquakes. The S waveforms of both the larger events and the EGF event were windowed to a length of 2 s, processed to remove the DC component, padded with zeroes to 1024 points, and then Fourier-tranformed to the frequency domain. The spectrum of each larger event was divided by that of the EGF event and then inverse-transformed to obtain the STF. To stabilize the deconvolution procedure, a Gaussian filter was used to slightly smooth the amplitude spectra before the spectral division. After deconvolution, a fourth-order Butterworth low-pass filter with a corner frequency of 30 Hz was used to reduce the high frequency noise. This noise may be caused by the variation of background noise at the stations, the spatial separation between the larger and EGF events, and the non-deltaness of the source time function of the EGF event (Frankel *et al.*, 1986; Li and Thurber, 1988). The retrieved STFs for the two larger events with magnitudes of 1.6 and 3.3 are depicted in Figure 7. The STF of the M1.6 event (920314-2128) is a simple pulse with a source duration of about 0.05 s. The STF of the M3.3 earthquake (920310-0545) appears to have two peaks, suggesting two episodes of rupture with a total duration of about 0.15 s. The S wave seismogram for the M3.3 earthquake is clearly more complex than those of the M1.6 and EGF events (Figure 7).

Three-component S waveforms of an EGF event (920311-0120, M0.2) recorded at four stations were deconvolved from those of an M1.6 earthquake (920314-2128) to extract the STFs for the larger event. The three-component seismograms and retrieved STFs are shown in Figure 8. The STFs obtained with different components at the same station are very similar and typically have only slight differences, suggesting that the assumption of a similar focal mechanism for the two events in the pair is correct. We summed the STFs extracted with three component data at a station and used the stack as an average estimate of the STF at that station. The procedure not only increases the signal-to-noise ratio for the STFs by a factor of 1.73, but also should average out the slight dissimilarity caused by the differences in location and focal mechanism between the EGF event and the larger event. In the following analysis, the retrieved STFs will be the stacked three-component average.

Table 2

First motion polarities of P and SH waves

Event ID	A11		A16		A21		A54		A61		A64	
	P	SH	P	SH	P	SH	P	SH	P	SH	P	SH
890210-0538	n	n	+	+	n	n	-	-	-	+	+	+
890915-0216	n	n	+	+	n	n	-	-	-	+	+	+
901021-1338	+	+	+	-	-	-	-	-	+	-	-	+
901102-0427	+	+	+	-	-	-	-	-	+	-	-	+
920310-0545a	-	-	-	-	-	+	-	-	-	+	+	-
920310-0545b*	-	-	-	-	-	+	-	-	-	+	+	-
920311-0120	n	n	-	-	+	+	-	-	-	+	+	-
920314-2128	-	-	-	-	+	+	-	-	-	+	+	-
890309-0941	-	-	+	-	n	n	-	-	-	-	-	+
890310-0329	n	n	+	-	n	n	-	-	-	-	-	+
890310-0451	n	n	+	-	n	n	-	-	-	-	-	+
890311-0831	-	-	+	-	n	n	-	-	-	-	-	+

*: A double event and polarities of the second event were based on cross-correlation analysis.

n: Data were not available or poor signal-to-noise ratio.

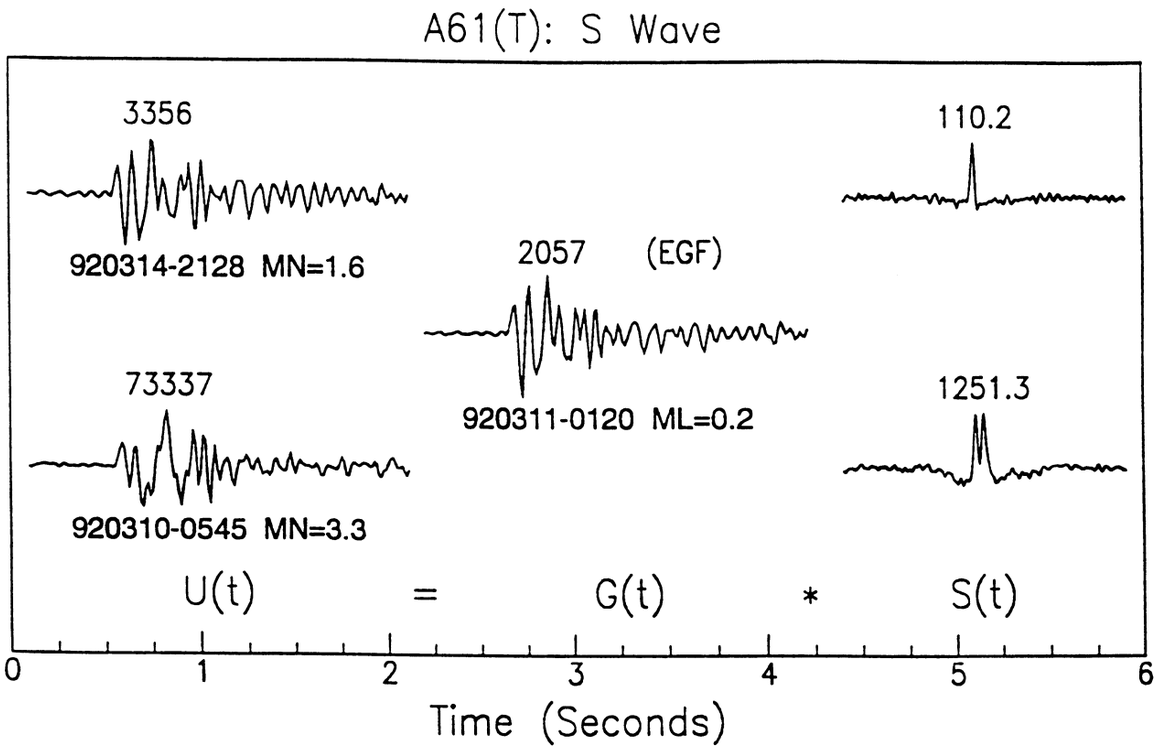

Figure 7. Demonstration of the EGF deconvolution procedure to retrieve the relative STFs of two larger earthquakes of a multiplet consisting of three events. The tangential S waveform of the smallest event is treated as the EGF and deconvolved from the seismograms of the two larger events,U(t), to derive the STFs, S(t), of the two larger earthquakes. The STF of the M3.3 earthquake has two distinct pulses implying two episodes of rupture during the event.

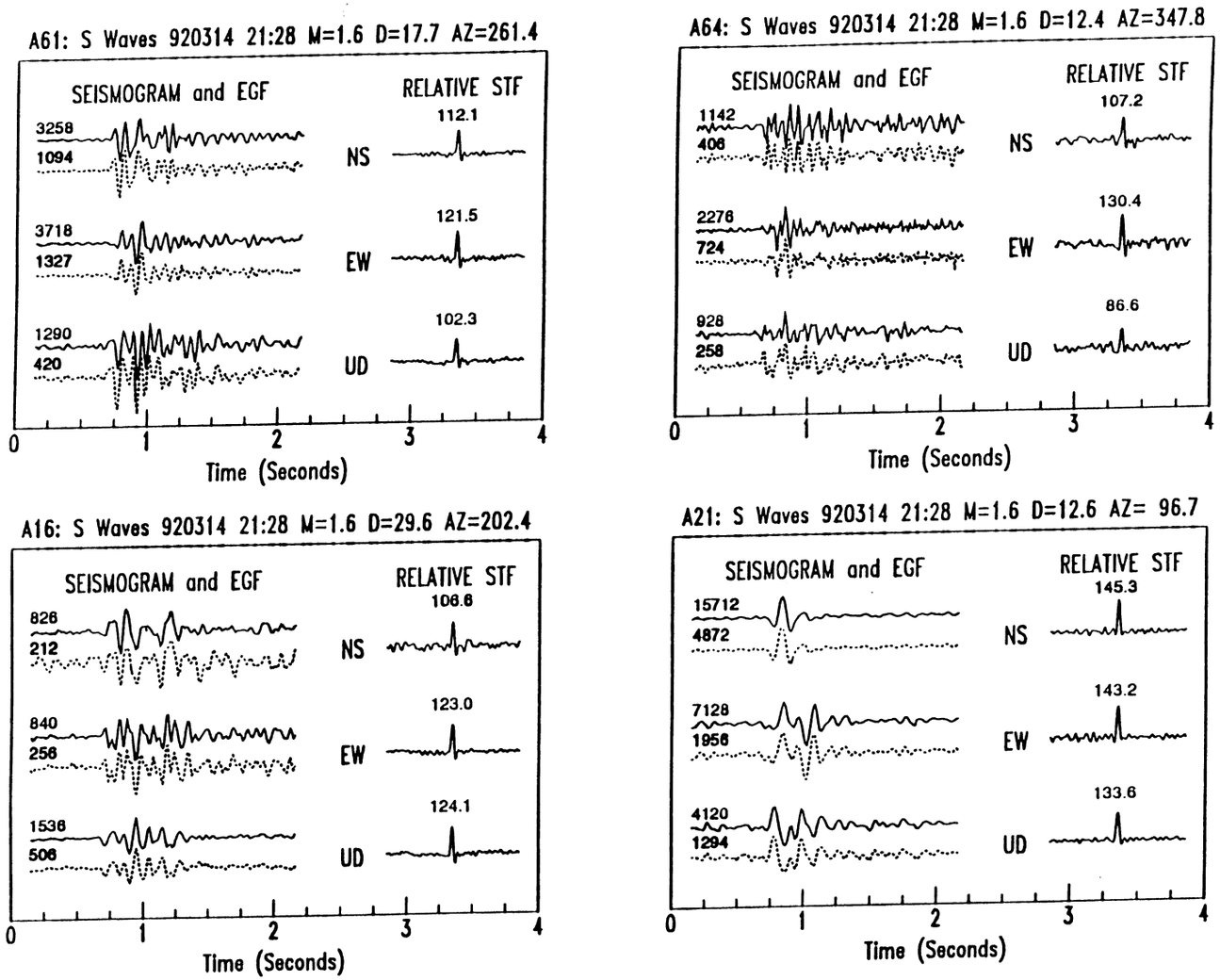

Figure 8. Three-component S waveforms of a main (solid line) and EGF (dotted line) event pair recorded at four CLTN stations, along with the STF estimates. STFs of the three components at each station are very similar and can be effectively stacked to enhance the signal-to-noise ratio of the source pulse and to average out minor dissimilarities which arise from slight differences in the focal mechanisms and locations of the main and EGF events.

SOURCE TIME FUNCTIONS AND RUPTURE DIRECTIVITY

The STFs of an M1.8 earthquake (890201-0538 from doublet 1 in Figure 3) were retrieved using three-component S wave seismograms of a nearby small event (890915-0216, M0.0) recorded at stations A16, A54 and A61 (Figure 9a) as the EGFs. The STF of the event (Figure 9b) consists of a simple pulse with a source duration of about 0.05 s. The pulse width shows little azimuthal dependence. The maximum pulse amplitude at station A61 is about 15% larger than those observed at stations A16 and A54, which are almost identical. We attribute the somewhat larger amplitude of the STF at station A61 to the relatively high noise level at that recording site (Figure 9b) rather than to rupture directivity. The lack of a significant azimuthal variation of the pulse width and amplitude suggests that the event can be charaterized as a point source.

Three-component S wave seismograms of a smaller event (901102-0427, M0.5) recorded at three stations (Figure 10a) were treated as the EGFs and deconvolved from the S waveforms of an M3.3 earthquake (901021-1338 from doublet 2 in Figure 3) to obtain the STFs (Figure 10b) of the larger event. The STFs show clearly the azimuthal variation of pulse amplitude and width, providing strong evidence for the rupture directivity of the earthquake. The STF pulse at station A16 has the largest amplitude and narrowest pulse width, while the STF pulse observed at station A11 has the smallest amplitude and widest pulse width. The azimuthal variation of the STF of the event indicates that the rupture propagated roughly towards station A16. Estimates of the rupture direction and rupture velocity from analysis of the STFs will be discussed next.

Theoretical studies (*e.g.*, Ben-Menahem, 1962) on the radiation of body waves from a finite moving seismic source predict the azimuthal dependence of STF amplitude and pulse width. For a unilaterally propagating rupture, the source duration is narrowest in the direction of rupture propagation and widest in the opposite direction. Due to the same effect, the amplitude of the STF in the rupture direction is larger than that in the opposite direction by a factor of $[1 + V_r/c]/[1- V_r/c]$ (Hirasawa and Stauder, 1965), where c and V_r are the velocities of the wave and the rupture, respectively. Although the direction of a propagating rupture can be inferred from the azimuthal dependence of the STF pulse width and amplitude, the poor time resolution (0.0125 s) of our data set prevents us from getting a reliable estimate of the rupture direction from the azimuthal variation of pulse width. Therefore, we used the azimuthal variation of the pulse amplitudes to estimate the rupture direction.

Savage (1965) studied the effect of rupture velocity upon the first motion amplitude and gave the modulating function F_1 for unilateral dislocation and F_2 for bilateral dislocation as

$$F_1 = V_r/[1-(V_r/c)\cos(\emptyset-\emptyset_0)] \quad (1)$$

$$F_2 = 2V_r/[1 - (V_r/c)^2\cos^2(\emptyset-\emptyset_0)], \quad (2)$$

where $\emptyset$ and $\emptyset_0$ are azimuths of a station and rupture direction, respectively. The reciprocal of the amplitude (1/A) can be written as

$$1/A_1 = K_1/F_1 = K_1[1/V_r - (1/c)\cos(\emptyset-\emptyset_0)] \quad (3)$$

$$1/A_2 = K_2/F_2 = K_2[1/V_r -(V_r/c)^2\cos^2(\emptyset-\emptyset_0)], \quad (4)$$

where K_1 and K_2 are constants. We can estimate the rupture direction $\emptyset_0$ by fitting the maximum amplitudes of the STFs at stations with different azimuths ($\emptyset$) to a straight line defined by

$$[1/A_i] = a_i - b_i [\cos^i(\emptyset-\emptyset_0)], \quad (5)$$

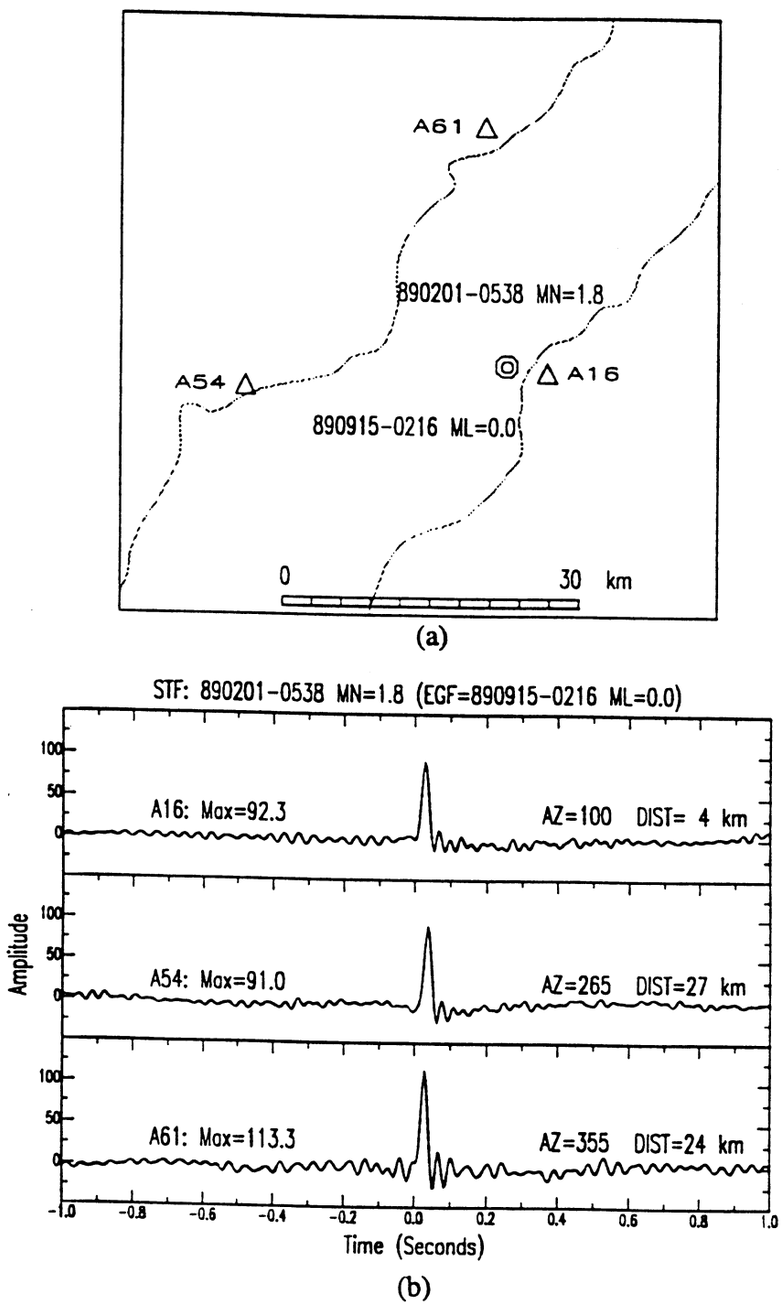

Figure 9. (a) Epicentral location of earthquake doublet 1 (M1.8 and M0.0) in the CSZ. (b) STFs of the M1.8 event derived for the three CLTN stations (triangles) in (a). No strong azimuthal variation in pulse amplitude or width is demonstrated by the STFs.

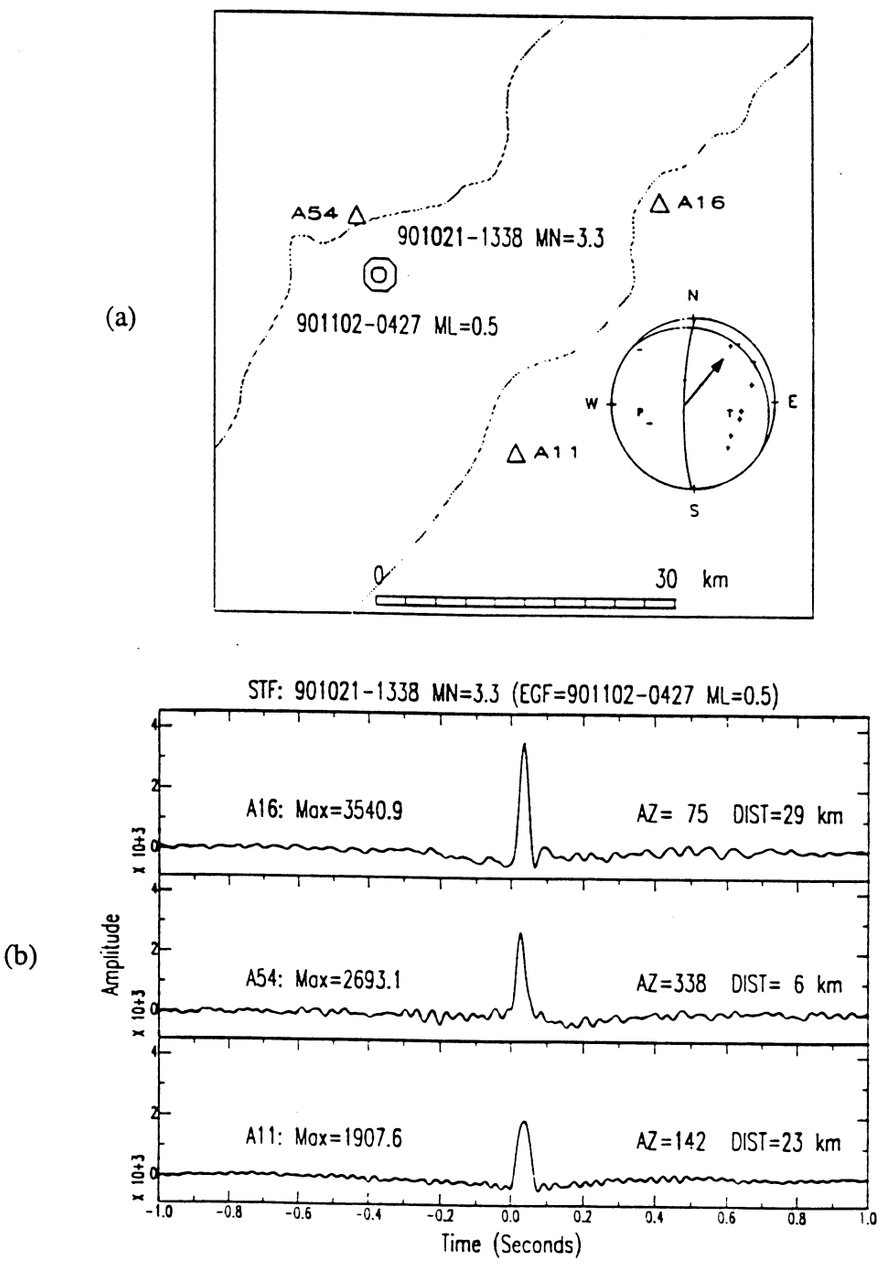

Figure 10. (a) Epicentral location of earthquake doublet 2 (M0.5 and M3.3) in the CSZ and the focal mechanism of the larger event. (b) STFs of the M3.3 event retrieved for the three CLTN stations (triangles) in (a). The effect of rupture directivity is observed in the large azimuthal variation in pulse amplitude and width of the STFs. The pattern of variation in the STF pulses indicates a rupture approximately toward station A16. The arrow in (a) points from the preferred fault plane in the rupture direction.

where i is 1 and 2 for unilateral and bilateral rupture, respectively. The slope b_i and intercept a_i of the straight line can be used to estimate the seismic Mach number,

$$V_r/c = b_1/a_1 = (b_2/a_2)^{1/2}. \quad (6)$$

We searched for the rupture direction $\emptyset_0$ by fitting the STF amplitudes A_i with a straight line defined by equation (5). The best fitting result for the 901021-1338 event is obtained for the case of i=1 (unilateral rupture), with the maximum correlation coefficient corresponding to an optimal rupture propagation direction of $\emptyset_0 = 40^\circ$ and $V_r = 0.5V_S$ (Figure 11a). The linear correlation coefficients are plotted as a function of the rupture direction $\emptyset_0$ in Figure 11b. The rupture direction in conjunction with the focal mechanism allow us to determine the actual fault plane of the event . Our inferred rupture direction is marked with an arrow on the preferred fault plane (Figure 10a).

STFs of three larger events (M4.3, M1.2 and M4.4) were retrieved using the smallest earthquake (890310-0451, M0.2) of multiplet 4 (Figure 3) as the EGF event. The STFs of each event recorded at three widely spaced stations show significant azimuthal variations (Figure 12). The amplitudes of the STF pulses for the M4.4 event increase as the azimuth increases (Figure 12d), with the smallest amplitude at station A16 and the largest amplitude at station A64, indicating that the rupture of the M4.4 event is towards station A64 (Figure 12a). For the M4.3 earthquake, the largest pulse amplitude and the narrowest pulse width of the STF is recorded at station A61 (Figure 12b) and indicates a rupture direction towards the west (Figure 12a). We even observed rupture directivity for the M1.2 event. The amplitudes of the STF pulses observed at stations A61 and A64 are larger than that for station A16 by a factor of 2 (Figure 12c), suggesting that the rupture direction of the earthquake is towards the northwest between stations A61 and A64 (Figure 12a).

We searched for the optimal rupture directions for the M4.3, M1.2 and M4.4 earthquakes by fitting a straight line to the STF amplitude data for each event as described in equation (5). The closest fits are obtained for unilateral ruptures and these are shown in Figures 13a, 13b and 13c. The rupture velocity for these events ranges from $0.5V_S$ to $0.7V_S$. The rupture directions for the M4.3, M1.2 and M4.4 earthquakes are estimated to be 290°, 300° and 320°, respectively, suggesting that the rupture direction of the earthquake multiplet rotated about 30° clockwise (Figure 13d). However, the reason for this apparent rotation of the rupture direction is not yet clear. The rupture directions of the three events are also consistent with the spatial trend of the relative locations of events in the multiplet (Figure 3). Based on the rupture directions and the focal mechanisms of the M4.3 and M4.4 events, we determined that the east-dipping planes were the actual fault planes of the two earthquakes and marked the rupture directions with arrows on these fault planes (Figure 12a). It is interesting to note that Wetmiller and Adams (1990) also selected the east-dipping planes as favorable fault planes for these events based on seismicity distribution and geological information.

The rupture directivities of M > 2.5 microearthquakes have been observed in California and Hawaii and used to infer the actual fault planes (*e.g,* Frankel *et al.*, 1986; Mori, 1993; Li and Thurber, 1988). In this study, we observed the rupture directivity even for an event with a magnitude as low as 1.2. This study as well as previous investigations have shown that the rupture directivities, along with the P focal mechanisms, can be used to determine which nodal plane is the actual fault plane. The focal mechanisms of microearthquakes in northeastern North America have been documented by many authors (*e.g.,* Pulli and Toksöz, 1981; Lamontagne, 1987; Adams *et al.*, 1988; Ebel and Bouck, 1988). Based on geological and seismicity information investigators can sometimes determine the preferred fault plane for an event, but for most events choosing the nodal plane which represents the actual fault plane is difficult. With the

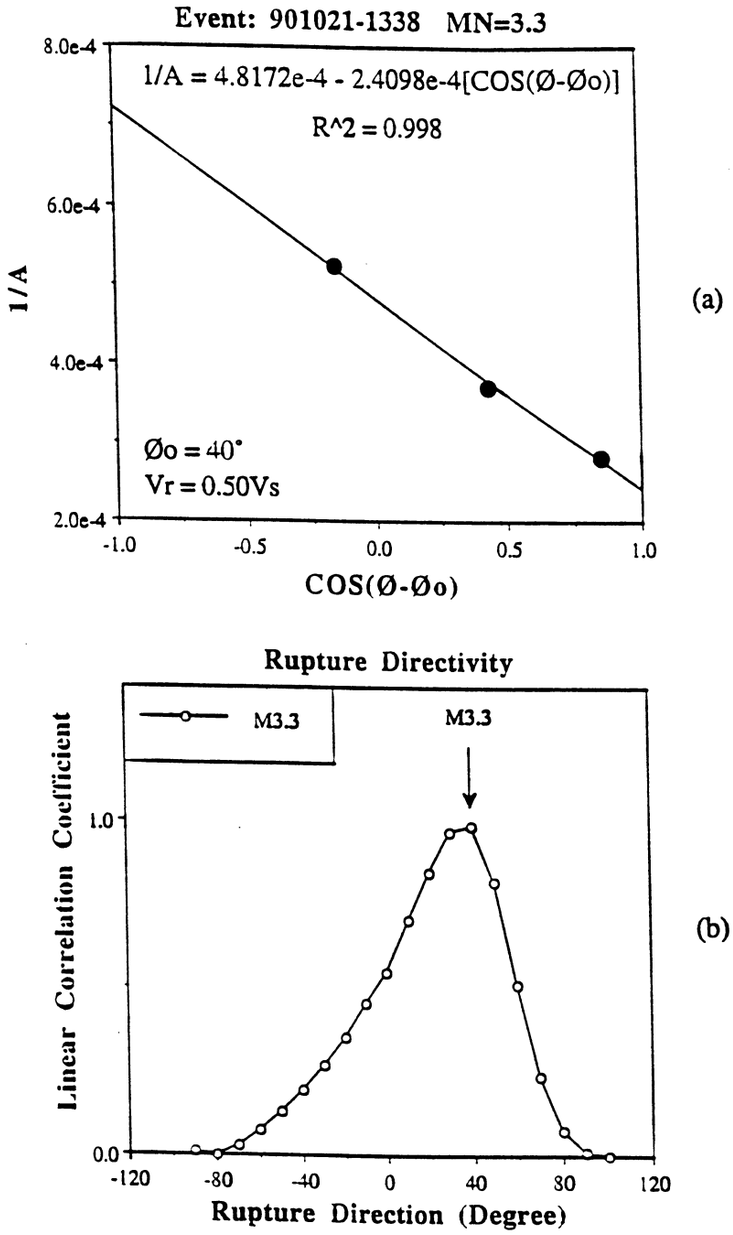

Figure 11. (a) Best straight-line fit of the peak amplitudes of the STF pulses for the main event in Figure 10a. The linear equation for this straight line has been used to derive the rupture direction $Ø_O$ and rupture velocity v_r . R is the correlation coefficient. (b) Linear correlation coefficients plotted as a function of the rupture direction. The peak correlation coefficient , corresponding to the best fit of the straight line to the amplitude data, occurs at a rupture direction of N40°E.

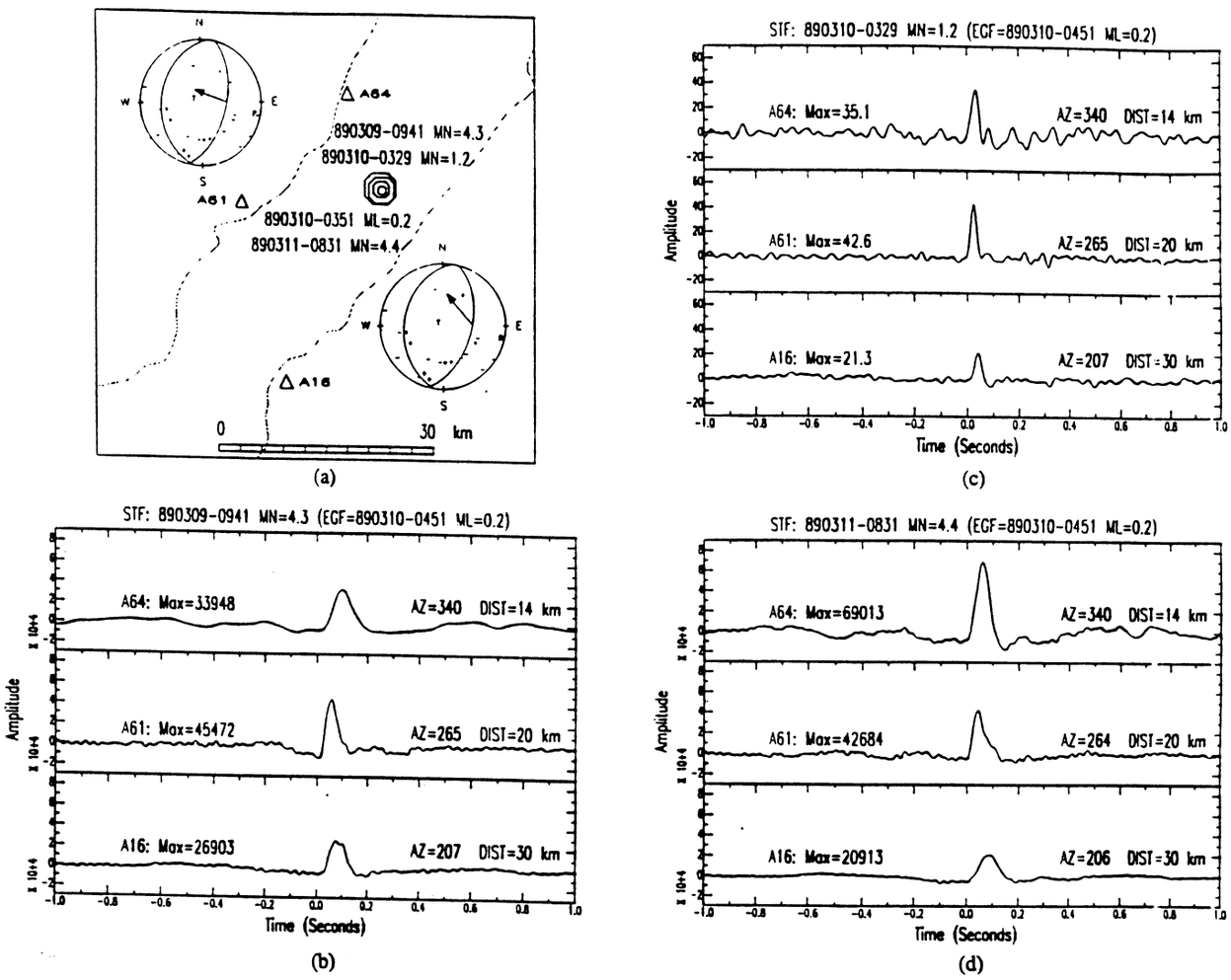

Figure 12. (a) Epicentral location of multiplet 4 (M0.2-4.4) and the focal mechanisms of the two largest events. (b-d) The STFs for the three larger earthquakes recorded at the three stations (triangles) in (a). All three events exhibit a clear rupture directivity revealed by the significant azimuthal variations in pulse amplitude and width of the STFs, indicating a rupture direction approximately northwest. The arrow points from the probable fault plane in the rupture direction on the thrust focal mechanisms of the M4.3 and M4.4 earthquakes in (a).

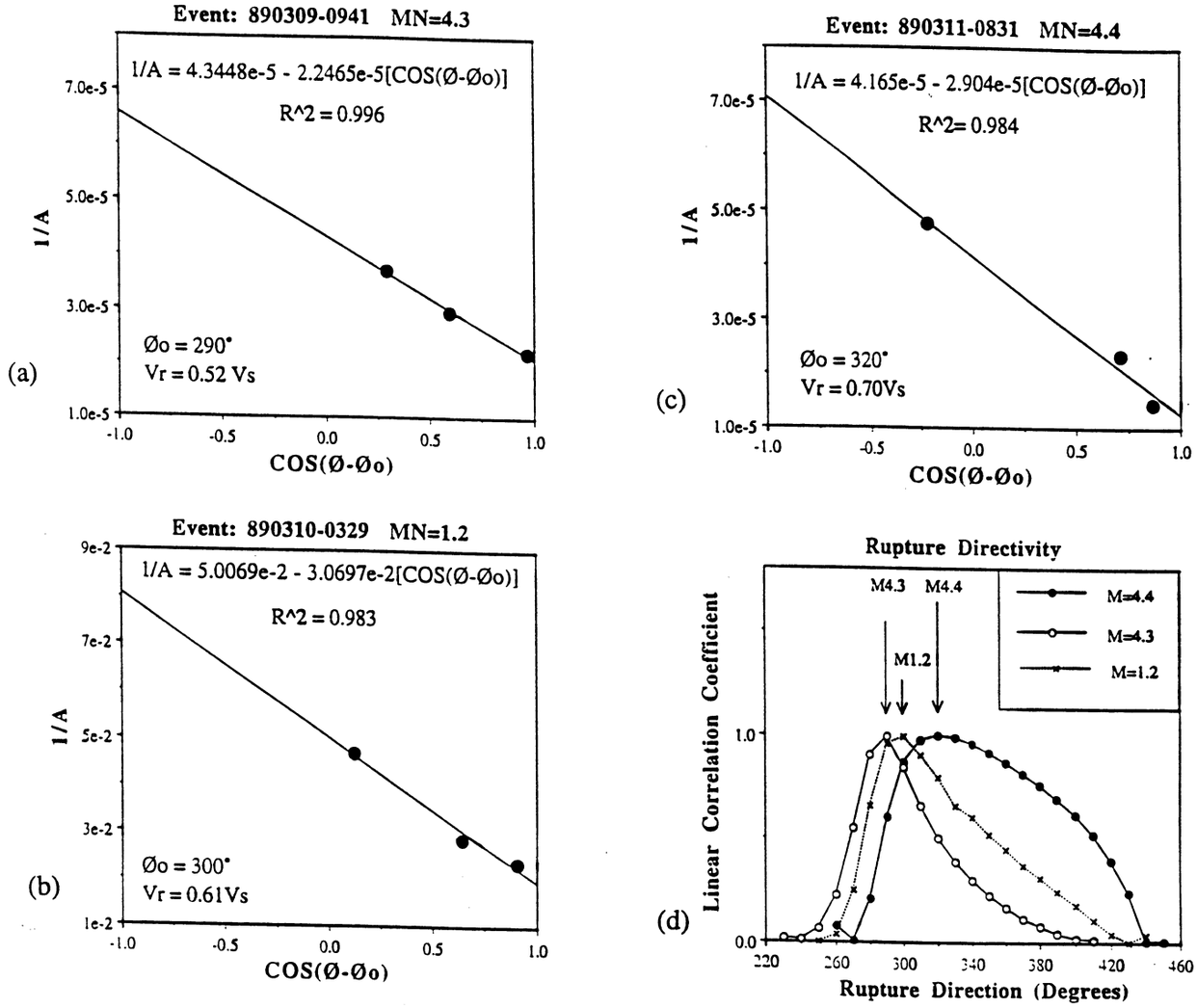

Figure 13. (a-c) Best straight-line fits of the peak amplitudes of the STF pulses at three CLTN stations for the three larger events of multiplet 4. The linear equation describing the straight line has been used to estimate the rupture directions ($Ø_O$) and velocities (v_r) of the three events. (d) The correlation coefficient is optimized (*i.e.*, best straight-line fit found) at rupture directions of 290°, 300°, and 320° for the M4.3, M1.2 and M4.4 earthquakes, respectively. Note the apparent clockwise rotation of the rupture directions.

method we present here and suitable earthquake pairs, it is possible to determine the actual fault planes for the larger events in the pairs.

RUPTURE COMPLEXITY

STFs of the 920310-0545 (M3.3) and the 920314-2128 (M1.6) events were extracted from seismic recordings at four stations (Figure 14a). S waveforms of the smallest event (920311-0120, M0.2) in the multiplet were used as the EGFs. The STF of the M1.6 earthquake is a simple pulse with a duration of about 0.05 s, and reveals no rupture directivity as evidenced by the lack of pulse amplitude and width variation at the different stations (Figure 14b). In contrast, the STF of the M3.3 event has two distinct peaks at three of the four stations, suggesting two episodes of rupture with a total duration of about 0.15 s (Figure 14c). Since the M1.6 event is simple with no rupture directivity, we substituted its waveforms for those of the M0.2 event as the EGFs. The STFs of the M3.3 earthquake show no change in relative pulse shape among the four stations (Figure 14d) despite changing the EGF event. This example demonstrates that the STF of a larger event can be successfully retrieved so long as one or more suitable EGF events can be found.

Although the STFs of the M3.3 earthquake indicate a rupture direction approximately east-west, the equation (5) we used to estimate the rupture direction is not appropriate for a double event. Therefore, we have to use other information to constrain the rupture direction and the actual fault plane. The relative locations of the two subevents (Figure 3) and the focal mechanism of the first subevent suggest rupturing towards the east with the west-dipping plane being the preferred fault plane. We marked the fault plane with an arrow on the focal mechanism solution of the first subevent in Figure 14a. Double events had previously been observed for relatively large earthquakes (M ~ 5) in northeastern North America (*e.g.*, Nabelek, 1984; Ebel *et al.*, 1986), but in this study we have found that even a small earthquake (M~3) may exhibit rupture complexity. The rupture complexities of microearthquakes in Miramichi, Canada (M=3-4.1) and in Reading, Pennsylvinia (January 16, 1994, M=4.6) were also observed from retrieved relative source time functions (Li *et al.*, 1994).

SOURCE PARAMETERS

We estimated the source parameters for the larger shocks of the doublets and multiplets in the CSZ. The seismic moment for the EGF event (M_{og}) in each group was calculated based on the low-frequency amplitudes of its S wave displacement spectrum Ω_o (Boatwright, 1980) as follows:

$$M_{og} = \frac{4\pi\Omega_o D}{FR}[\rho(s)\rho(r)c(r)]^{1/2}[c(s)]^{5/2}, \qquad (7)$$

where $\rho(s) = 2.8$ and $\rho(r) = 2.3$ g/cm^3 are the densities at the source and receiver, respectively, $c(s) = 3.6$ and $c(r) = 2.3$ km/s are the S wave velocities at the source and receiver, respectively, D is the epicentral distance, F is the free surface correction at the receiver, and R is the radiation pattern. It is assumed that the EGF event had a focal mechanism similar to that of the larger event. Since no focal mechanism is available for the M1.8 earthquake (890201-0538), no radiation pattern correction is made for this event. The seismic moments of larger events (M_o) are estimated by $M_o = AM_{og}$, where A is the area under the STF.

The rise times ($\tau_{1/2}$) were measured from STFs at different stations and averaged to estimate the fault radius using the relationship given by Boatright (1980) for a circular source,

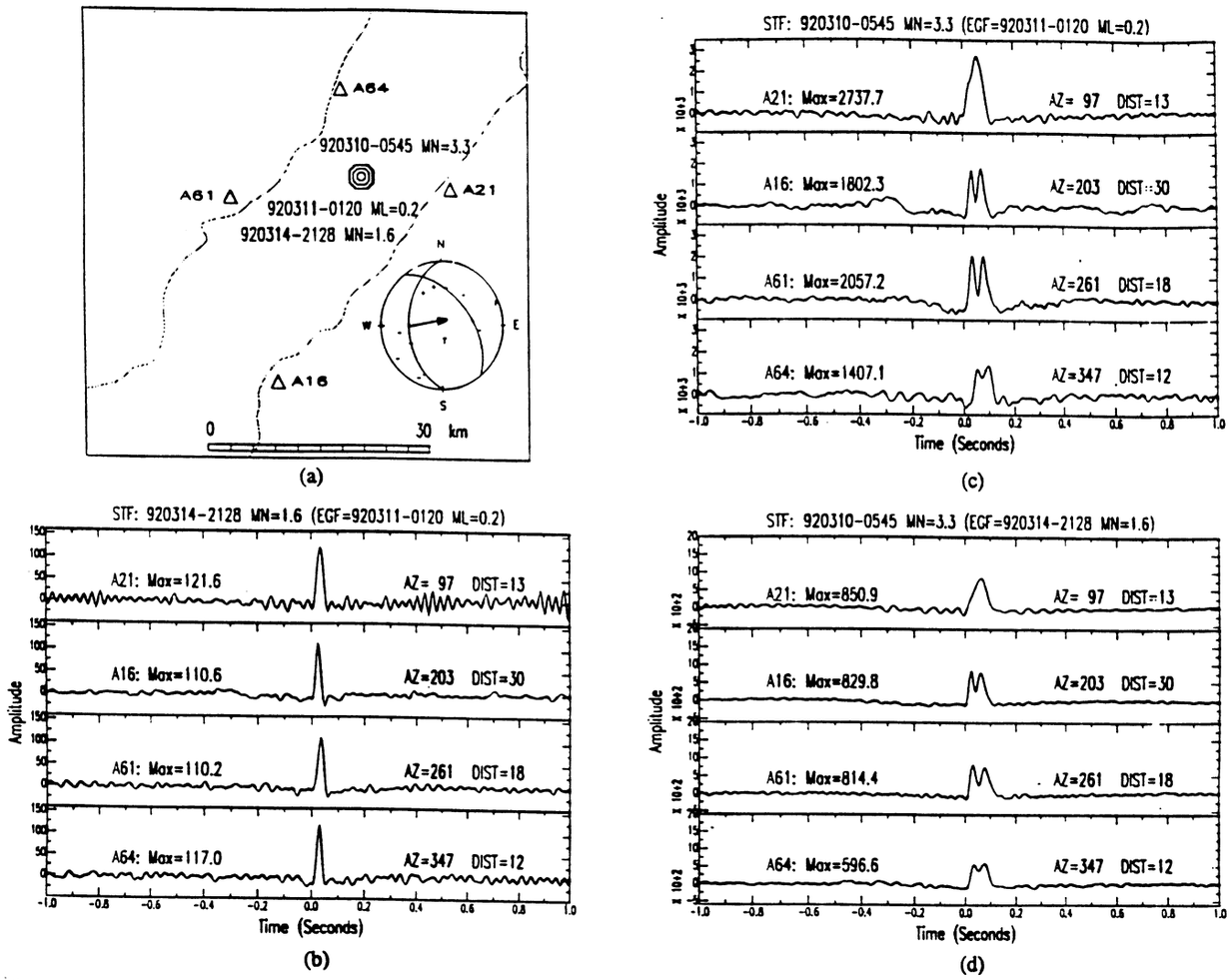

Figure 14. (a) Epicentral location of multiplet 3 (M0.2-3.3) and the focal mechanism of the largest event. (b-d) STFs of the M1.6 and M3.3 events derived at the four CLTN stations (triangles) in (a). The M0.2 earthquake is used as the EGF to retrieve the STFs in (b) and (c). STFs of the M3.3 event were also estimated with the M1.6 event as the EGF in (d). The pulse shape is preserved among the STFs of the four stations when compared to the results obtained using the M0.2 event as the EGF in (c). The azimuthal variations of the STF pulse amplitudes and widths suggest a rupture approximately from west to east. The arrow extends from the probable fault plane on the thrust focal mechanism (first subevent) toward the direction of rupture.

$$r = \frac{\tau_{1/2} v_r}{[1-(v_r \sin\theta/c)]}, \quad (8)$$

where c and V_r are the velocities of the wave and rupture, respectively, and θ is the take-off angle. The rupture velocity is assumed to be 0.75 times the shear-wave velocity or 2.7 km/s and $\theta = 45°$. The static stress drop ($\Delta\sigma$) is determined from the seismic moment and fault radius using Brune's (1970) formula

$$\Delta\sigma = \frac{7M_o}{16r^3}. \quad (9)$$

The calculated source parameters (seismic moment, fault radius and stress drop) are summarized in Table 3. Because of the relatively short duration of the STFs of the events and the cubic dependence of the stress drop on the rise time, a small error in the rise time measurement will result in a very large error in the estimate of stress drop (Table 3), especially for those events with smaller magnitudes and extremely short durations (*i.e.*, M1.2-1.8). These large errors reflect the difficulty in making accurate measurements of the stress drops for small events.

For M3.3 to 4.4 events (M_O = 1.4x10^{20} to 5.3x10^{21} dyne-cm), the stress drop estimates range from 24 to 90 bars and the fault radii are from 120 to 330 m. We have compared our estimates of source parameters with those obtained by other investigators for earthquakes in the CSZ (Table 3). Boatwright (1994) and Atkinson and Somerville (1994) estimated stress drops of 50 to 70 bars and fault radii of 200 to 350 m for three earthquakes in the magnitude range of 3 to 4.5. These results agree quite well with the source parameters we estimated using the EGF method.

For smaller events with magnitudes 1.2 to 1.8 (M_O = 3.5x10^{18} to 7.2x10^{18} dyne-cm), the stress drops fall to 2 to 3 bars. There is an apparent correlation of the stress drop with the seismic moment (Figure 15a). An empirical relationship based on eight data points was obtained as $\text{Log}(\Delta\sigma) = -9.7 + 0.5422\text{Log}(Mo)$. The dependence of stress drop on the size of an earthquake has been observed by other researchers (Boatwright, 1994; Shi *et al.*, 1994) for earthquakes in northeastern North America. Our estimates of stress drop increase with earthquake size in a manner consistent with the stress drop scaling observed by Boatwright (1994) for 97 earthquakes in northeastern North America (Figure 15b). However, Feng and Ebel (1993) found no scaling relationship between the stress drop and earthquake size for 12 small events located in New England. Due to the relatively large errors associated with the stress drop estimates we derived for the smaller events and the limited data set, we suggest that further investigation using waveform data of more events with better time resolution (high sampling rate) is required to verify the apparent scaling relationship between stress drop and seismic moment.

CONCLUSIONS

In this study the EGF technique has been successfully applied to retrieve the relative source time functions (STFs) of seven larger microearthquakes, ranging in magnitude from 1.2 to 4.4 and including three events less than magnitude 2. The STFs reveal that six of the events are simple with a single pulse ranging in source duration from 0.05 to 0.2 s. The azimuthal variation in amplitude observed in the STFs indicates definite rupture directions for five of the events, including one with magnitude only 1.2. The rupture velocities derived for these events vary from $0.5V_S$ to $0.7V_S$. In addition to this, the STF of one event (M3.3) displays two distinct pulses, suggesting a complex source process with two episodes of rupturing. These results show that

Table 3

Source parameters for earthquakes in the CSZ

Event ID	Magnitude M_N or (M_L)	M_{og} 10^{18} (dyne-cm)	M_o/M_{og}	M_o 10^{19} (dyne-cm)	rise time $\tau_{1/2}$ (ms)	radius r (m)	Stress drop $\Delta\sigma$ (bars)
890915-0216	(0.0)	1.6					
890201-0538	1.8		2.2	0.352	16.7± 7.2	96± 44	1.7 (0.6-10.9)
901102-0427	(0.5)	3.8					
901021-1338	3.3		82	31.16	25.0±12.5	143± 72	46.6 (13.7-381)
920311-0122	(0.2)	1.8					
920310-0545a	3.3		75	13.50	21.9± 6.3	125± 36	30.2 (14.2-83.3)
920310-0545b			90	16.20	25.0±12.5	143± 72	24.2 (7.1-198)
920314-2128	1.6		4	0.720	18.8± 7.2	108± 44	2.5 (0.9 -12.0)
890310-0451	(0.2)	2.0					
890309-0941	4.3		2415	483.0	50.0±12.5	286± 72	90.3 (46.1-216)
890310-0329	1.2		1.8	0.360	16.7± 7.2	96 ± 44	1.8 (0.6-11.2)
890311-0831	4.4		2651	530.2	58.3±19.1	334±109	62.3 (26.7-204)
		*	*	*	*	*	*	
March 1, 1925	m_b = 6.5	Ebel *et al.* (1986)					100 - 300
		Bent (1992)					35
August 19, 1979	m_b = 5.0	Hasegawa and Wetmiller (1980)					50
March 9, 1989	M_N = 4.3	Boatright (1994)				340	50
March 3, 1990	M_N = 3.6	Boatright (1994)				210	69
March 3, 1990	M_N = 3.6	Atkinson and Somerville (1994)					70

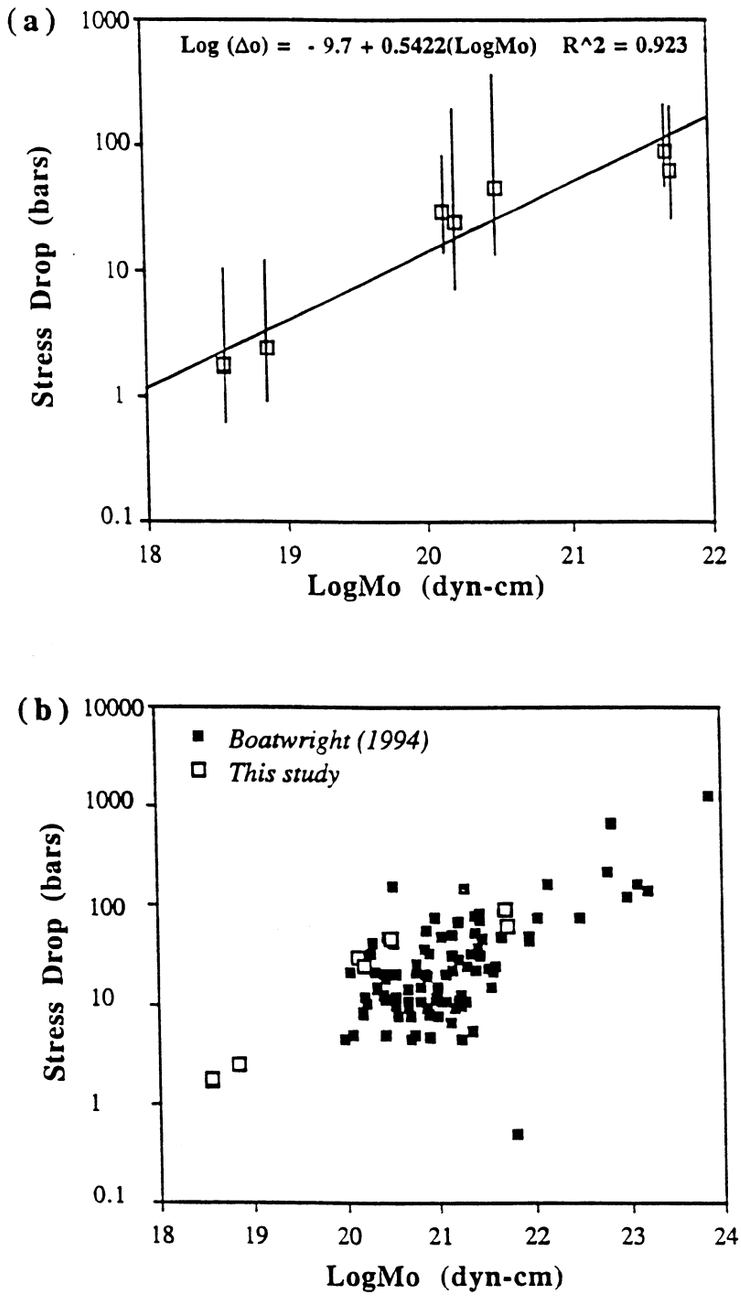

Figure 15. (a) Stress drops estimated for the seven target events (including one double event) in this study plotted versus seismic moment. The slope of the line fitted to the data describes an apparent scaling of stress drop to earthquake size. (b) Stress drops estimated in this study and those of 97 northeastern North American earthquakes analyzed by Boatwright (1994) plotted versus seismic moment. The apparent stress drop scaling between the two data sets is consistent.

even microearthquakes in northeastern North America may exhibit a complex rupture and rupture directivity. Estimates of the rupture direction were incorporated with P wave focal mechanisms to infer the actual fault planes of the four largest earthquakes.

The source parameters estimated from the derived STFs vary from 3.5×10^{18} to 5.3×10^{21} dyne-cm for seismic moment, from 96 to 334 meters for fault radius, and from 2 to 90 bars for stress drop. These estimates agree well with values for earthquakes in the CSZ obtained by other researchers using different methods (Hasegawa and Wetmiller, 1980; Boatwright, 1994; Atkinson and Somerville, 1994). The stress drops estimated in this and other studies of earthquakes in northeastern North America show an apparent wide variation (Hasegawa and Wetmiller, 1980; Choy *et al.*, 1983; Nabelek, 1984; Ebel *et al.*, 1986; Somerville *et al.*, 1987; Nabelek and Suarez, 1989; Bent, 1992; Atkinson and Somerville, 1994; Boatwright, 1994). Moreover, the results of this study suggest an apparent scaling of stress drop to earthquake size. Our estimates of stress drop increase with earthquake size in a manner consistent with the stress drop scaling observed by Boatwright (1994) for 97 earthquakes in northeastern North America.

ACKNOWLEDGEMENT

We would like to thank the Geophysics Division of the Canadian Geological Survey (CGS) for the use of their seismic data. Without the continuous effort of data collection by the staff of the CGS, this research would not have been possible. In particular, we are indebted to Dr. R. North, W. Shannon, J. Drysdale and W. McNeil for their generous assistance in making the data available to us. We also thank J. Adams, R. Wetmiller, and M. Lamontagne for providing us with their reprints. We benefitted greatly from discussions with J. Adams, R. Wheeler, J. Ebel, R. Wetmiller and A. Bent. We want to express our appreciation to J. Ebel for providing us with additional waveform data recorded by the Weston Observatory of Boston College. J. Ebel and J. Zhang supplied the programs to compute and plot the focal mechanisms. This research was sponsored by the United States Geological Survey, Grant #1434-94-G-2421, under the National Earthquake Hazards Reduction Program.

REFERENCES

Adams, J., J. Sharp and M. Stagg (1988). New Focal mechanisms for southeastern Canada earthquakes, *Geological Survey of Canada, Open File 1892,* 109 pp.

Anglin, F.M. (1984). Seismicity and faulting in the Charlevoix zone of the St. Lawrence Valley, *Bull. Seism. Soc. Am., 74,* 596-603.

Atkinson, G.M. and P.G. Somerville, 1994. Calibration of time history simulation methods, *Bull. Seism. Soc. Am., 84,* 400-414.

Ben-Menahem, A. (1962). Radiation of seismic body waves from a finite moving source in the earth, *J. Geophys. Res., 67,* 345-350.

Bent, A. L. (1992). A re-examination of the 1925 Charlexoix, Quebec earthquake, *Bull. Seism. Soc. Am., 82,* 2097-2113.

Boatwright , J. (1980). A spectral theory for circular seismic sources: simple estimates of source dimension, dynamic stress drop, and radiated energy, *Bull. Seism. Soc. Am., 70,* 1-28.

Boatwright, J. (1994). Regional propagation characteristics and source parameters of earthquakes in northeastern North America, *Bull. Seism. Soc. Am., 84,* 1-15.

Brune, J.N. (1970). Tectonic stress and the spectra of seismic shear waves from earthquakes, *J. Geophys. Res., 75,* 4997-5009.

Buchbinder, G.G.R., A. Lambert, R.D. Kurtz, D. R. Bower, F.M. Anglin, and J. Peters (1988). Twelve years of geophysical research in the Charlevoix seismic zone, *Tectonophysics, 156,* 193-224.

Chen, Y.T., J.Y. Zhou, and J.C. Ni (1991). Inversion of near-source-broadband accelerograms for the earthquake source-time function, *Tectonophysics, 197,* 89-98.

Choy, G., J. Boatwright, J.W. Dewey and S.A. Sipkin (1983). A teleseismic analysis of the New Brunswick earthquake of January 9, 1982, *J. Geophys Res., 88,* 2199-2212.

Ebel, J.E. (1982). M_L measurements for northeastern United States earthquakes, *Bull. Seism. Soc. Am., 72,* 1367-1378.

Ebel, J.E., P.G. Somerville and J.D. McIver (1986). A study of the source parameters of some large earthquakes of northeastern North America, *J. Geophys Res., 91,* 8231-8247.

Ebel, J.E. and B.R. Bouck (1988). New focal mechanisms for the New England region: Constraints for the regional stress regime, *Seism. Res. Lett., 59,* 183-187.

Feng, Q. and J.E. Ebel (1993). Determination of rupture duration and stress drop for earthquakes in New England, *Seism. Res. Lett., 64,* 259.

Frankel, A. (1982). Precursors to a magnitude 4.8 earthquake in the Virgin Islands: spatial clustering of small earthquakes, anomalous focal mechanisms and earthquake doublets, *Bull. Seism. Soc. Am., 72,* 1277-1294.

Frankel, A., J. Fletcher, F. Vernon, L. Haar, J. Berge, T. Hanks and J. Burne (1986). Rupture characteristics and tomographic source imaging of M_L~3 earthquakes near Anza, southern California, *J. Geophys. Res., 91,* 12633-12650.

Fremont, M. and S. Malone (1987). High precison relative locations of earthquakes at Mount St. Helens, Washington, *J. Geophys. Res., 92,* 10223-10233.

Guinn, S. and L.T. Long (1977). A computer method for determination of valid focal mechanisms using P-wave first motions, *Earthquake Notes, 48,* 21-33.

Hartzell, S. (1978). Earthquake aftershocks as Green's functions, *Geophys. Res. Lett., 5,* 1-4.

Hasegawa, H.S. and R.J. Wetmiller (1980). The Charlevoix earthquake of 19 August 1979 and its seismo-tectonic environment, *Earthquake Notes, 51*, 23-37.

Hirasawa, T. and W. Stauder (1965). On the seismic body waves from a finite moving source, *Bull. Seism. Soc. Am., 55,* 237-262.

Hodgson, E.A. (1950). The Saint Lawrence earthquake March 1, 1925, *Pub. Dominion Obs. Ottawa, 7,* 363-436.

Hough, S.E., L. Seeber, A. Lerner-Lam and J.G. Armbruster (1991). Empirical Green's function analysis of Loma Prieta aftershocks, *Bull. Seism. Soc. Am., 815,* 1737-1753.

Hutchings, L. and F. Wu (1990). Empirical Green's functions from small earthquakes: A waveform study of locally recorded aftershocks of the 1971 San Fernando earthquake, *J. Geophys. Res., 95,* 1187-1214.

Ito, A. (1985). High-resolution relative hypocenters of similar earthquakes by cross-spectral analysis method, *J. Phys. Earth, 33,* 279-294.

Jordan, T.H. and K.A. Sverdrup (1981). Teleseismic location techniques and their application to earthquake clusters in the South-Central Pacific, *Bull. Seism. Soc. Am., 71,* 1105-1130.

Lamontagne, M. (1987). Seismic activity and structural features in the Charlevoix region, Quebec, *Can. J. Earth Sci. 24,* 2118-2129.

Li, Y., C. Doll and M.N. Toksöz (1994). Estimates of source time functions an associated parameters using the EGF method for the M=1.5 to 4.5 earthquakes in the Charlevoix, Miramichi, and New Hampshire seismic zones, *Seism. Res. Lett., 65,* 32.

Li, Y. and C.H. Thurber (1988). Source properties of two microearthquakes in Kilauea volcano, Hawaii, *Bull. Seism. Soc. Am., 78,* 1123-1132.

Mori, J. (1993). Fault plane determinations for three small earthquakes along the San Jacinto fault California: Search for cross faults, *J. Geophys. Res., 98,* 17711-17722.

Mori, J. and A. Frankel (1990). Source parameters for small events associated with the 1986 North Palm Springs, California, earthquake determined using empirical Green's functions, *Bull. Seism. Soc. Am., 80,* 278-295.

Mori, J. and S. Hartzell (1990). Source inversion of the 1988 Upland, California earthquake: determination of a fault plane for a small event, *Bull. Seism. Soc. Am., 80,* 507-518.

Mueller, C. (1985). Source pulse enhancement by deconvolution of an empirical Green's function, *Geophys. Res. Lett., 12*, 33-36.

Nabelek, J.L. (1984). Determination of earthquake source parameters from inversion of body waves, *Ph.D. Thesis*, Massachusetts Institute of Technology.

Nabelek, J. and G. Suarez (1989). The 1983 Goodnow earthquake in the central Adirondacks, New York: Rupture of a simple, circular crack, *Bull. Seism. Soc. Am.*, 79, 1762-1777.

Pechmann, J.C. and H. Kanamori (1982). Waveforms and spectra of preshocks and aftershocks of the 1979 Imperial Valley, California, earthquake: Evidence of fault heterogeneity?, *J. Geophys. Res., 87,* 10579-10597.

Poupinet, G., W.L. Ellsworth and J. Frechet (1984). Monitoring velocity variations in the crust using earthquake doublets: An application to the Calaveras fault, California, *J. Geophys. Res., 89,* 5719-5731.

Pulli, J.J. and M.N. Toksöz (1981). Fault plane solutions for northeastern United States earthquakes, *Bull. Seism. Soc. Am., 71*, 1875-1882.

Savage, J.C. (1965). The effect of rupture velocity upon seismic first motions, *Bull. Seism. Soc. Am., 55,* 263-275.

Shi, J., W.Y. Kim and P.G. Richards (1994). Estimation of seismic energy release, stress drop and determination of magnitude, for small regional earthquakes in the Northeastern U.S., *EOS, Trans., AGU, 75, no. 16,* 237.

Smith, W.E.T. (1962). Earthquakes of eastern Canada and adjacent areas 1534-1927, *Pub. Dominion Obs., 26,* 271-301.

Somerville, P.G., J.P. McLaren, L.V. LeFevre, R.W. Burger and D.V. Helmberger (1987). Comparison of source scaling relations of eastern and western North American earthquakes. *Bull. Seism. Soc. Am., 77*, 322-346.

Stevens, A. E. (1980). Reexamination of some larger La Malbaie, Quebec earthquakes (1924-1978), *Bull. Seism. Soc. Am., 70*, 529-557.

Tapley, W.C. and J.E. Tull (1991). SAC (Seismic Analysis Code), Users manual, Lawrence Livermore National Laboratory, Livermore, California.

Thorbjarnadottir, B.S. and J.C. Pechmann (1987). Constraint on relative earthquake locations from cross-correlation of waveforms, *Bull. Seism. Soc. Am., 77,* 1626-1634.

Wetmiller, R.J. and J. Adams (1990). An earthquake doublet in the Charlevoix seismic zone, Quebec, in *Current Research, Part B, Geological Survey of Canada, Paper 90-1*, 105-113.

Xie, J., Z. Liu, R. Herrmann and E. Cranswick (1991). Source processes of three aftershocks of the 1983 Goodnow, New York, earthquake: High-resolution images of small, symmetric ruptures, *Bull. Seism. Soc. Am., 81,* 818-843.

CHAPTER 2

CHARACTERIZING SEISMICITY AND ITS GEOLOGICAL ASSOCIATION IN THE CHARLEVOIX SEISMIC ZONE, QUEBEC, CANADA USING A RELATIVE LOCATION TECHNIQUE

YINGPING LI, CHARLES DOLL, JR., AND M. N. TOKSÖZ

Earth Resources Laboratory

Department of Earth, Atmospheric, and Planetary Sciences

Massachusetts Institute of Technology

Cambridge, MA 02139

Tel: (617)-253-7796

Fax: (617)-253-6385

Final Report to the United States Geological Survey

May 3, 1995

ABSTRACT

Precise locations of earthquakes are essential to characterizing an active fault. Well defined spatial patterns of seismicity, resulting from high-accuracy determinations of hypocenters, may be used to define the orientation and dimensions of a causative structure. In this study we have applied a waveform correlation and relative event location method to digitally recorded earthquakes in the Charlevoix Seismic Zone (CSZ) of Quebec, Canada to obtain high-precision locations for a large number of events. The purpose of this relocation effort is to attempt to produce well resolved spatial patterns of hypocenters which might delineate active faults in 3-D. Our results indicate that, in cross-section, the relocated hypocenters clearly define a V-shaped seismic zone striking northeast which appears to plunge at a shallow angle to the northeast. Along the northwest side of the St. Lawrence River in the CSZ, a strong spatial correlation is found between hypocenters determined by the relative event location method and some mapped faults striking northeast parallel to the river. In cross-section, these hypocenters define two vertically dipping planer features best resolved at a strike agreeing with crack orientations inferred from shear-wave splitting results. Other cross-sections of the data suggest alignments of hypocenters striking approximately northwest and extending from the northwest side across the river. These features may delineate active cross faults intersecting the long, northeast trending faults along the northwest side and in the river. Crack orientations determined from S polarization angles of a few earthquakes are consistent with the approximately northwest strike of one such feature in the southwest part of the CSZ. Cross faults could act as barriers preventing a potential rupture over the entire length of the CSZ along one of the northeast trending faults. The largest earthquake possible in the CSZ would depend on the maximum fault length capable of rupture.

INTRODUCTION

The goal of this part of the study is to relocate a substantial number of digitally recorded earthquakes in the Charlevoix Seismic Zone (CSZ) of Quebec and search for well defined patterns of hypocenters which may delineate active faults. In this approach, waveform correlation and relative event location methods are applied to waveform data to relocate the seismicity in the CSZ. The spatial patterns of the relocated seismicity are correlated with known geologic structures in the study area and other geophysical data to attempt to characterize active fault segments in detail. A well resolved spatial distribution of hypocenters can be used to ascertain the orientation and dimensions of an active fault.

Hypocenters of earthquakes are typically located using a computer program (e.g., HYPOINVERSE, Klein, 1978) applied to absolute arrival times picked from individual seismograms. The accuracy of the hypocenter solution is dependent on the interpretational bias of the record analyst picking the phase arrival times and on how well the crustal velocity model approximates the earth structure between the earthquake source and the recording station. Relative event location, the approach used in this study, is one alternative which produces more precise estimates of hypocentral locations of earthquake clusters, based on differential phase arrival times between events. Differential arrival times determined from waveform correlation analysis are typically more accurate than absolute picked times and provide valuable constraints on the relative locations among a cluster of events. Accordingly, a systematic relocation of hypocenters based on differential time data can be expected to yield clearer and tighter spatial patterns of seismicity.

Well resolved spatial distributions of seismicity in three dimensions may indicate whether earthquakes occur along shorter discontinuous fault segments as evidenced by isolated tight clusters of events, or along a longer continuous feature delineated by a longer seismic lineation of uniform event density. Differentiation between such types of seismicity patterns has important implications for estimating fault size and the maximum magnitude event associated with it. Moreover, the spatial distribution of the earthquakes and their associated stress drops helps to constrain the mechanical properties of faults correlated with the seismicity.

Charlevoix Seismic Zone and Network Data

The Charlevoix Seismic Zone (CSZ) is defined as an 80 x 35 km area located along the St. Lawrence River (Figure 1) in southern Quebec and is among the most seismically active zones (Figure 2) in eastern North America (Buchbinder *et al.*, 1988). Historically, the CSZ has been the location of several large earthquakes (Smith, 1962). The largest instrumentally recorded earthquake of this group occurred on March 1, 1925 with m_b = 6.5 (Stevens, 1980; Ebel *et al.*, 1986; Bent, 1992). The latest potentially damaging earthquake (m_b = 5) occurred on August 19, 1979 (Hasegawa and Wetmiller, 1980).

The waveform data used in this study were recorded by the Charlevoix Telemetered Network (CLTN) operated by the Geological Survey of Canada (GSC). The Geophysics Division of the GSC provided access to their database and the computer programs necessary to convert the waveform data from their in-house format to SAC, the data processing format used in this study. The CLTN consists of six three-component stations located in groups of three each along the northwest and southeast shorelines of the St. Lawrence River (Figures 1 and 2). These stations are situated parallel to the general northeasterly strike and bound the seismicity of the CSZ (Buchbinder *et al.*, 1988). The CLTN is a short-period local network which was modernized in November 1987 to include digital recording at a rate of 80 sps and three-component instruments with automatic gain control to insure a wide dynamic range of 126 dB (Munro, personal communication). The wide dynamic range of the instrument allows recording of M0-5 earthquakes

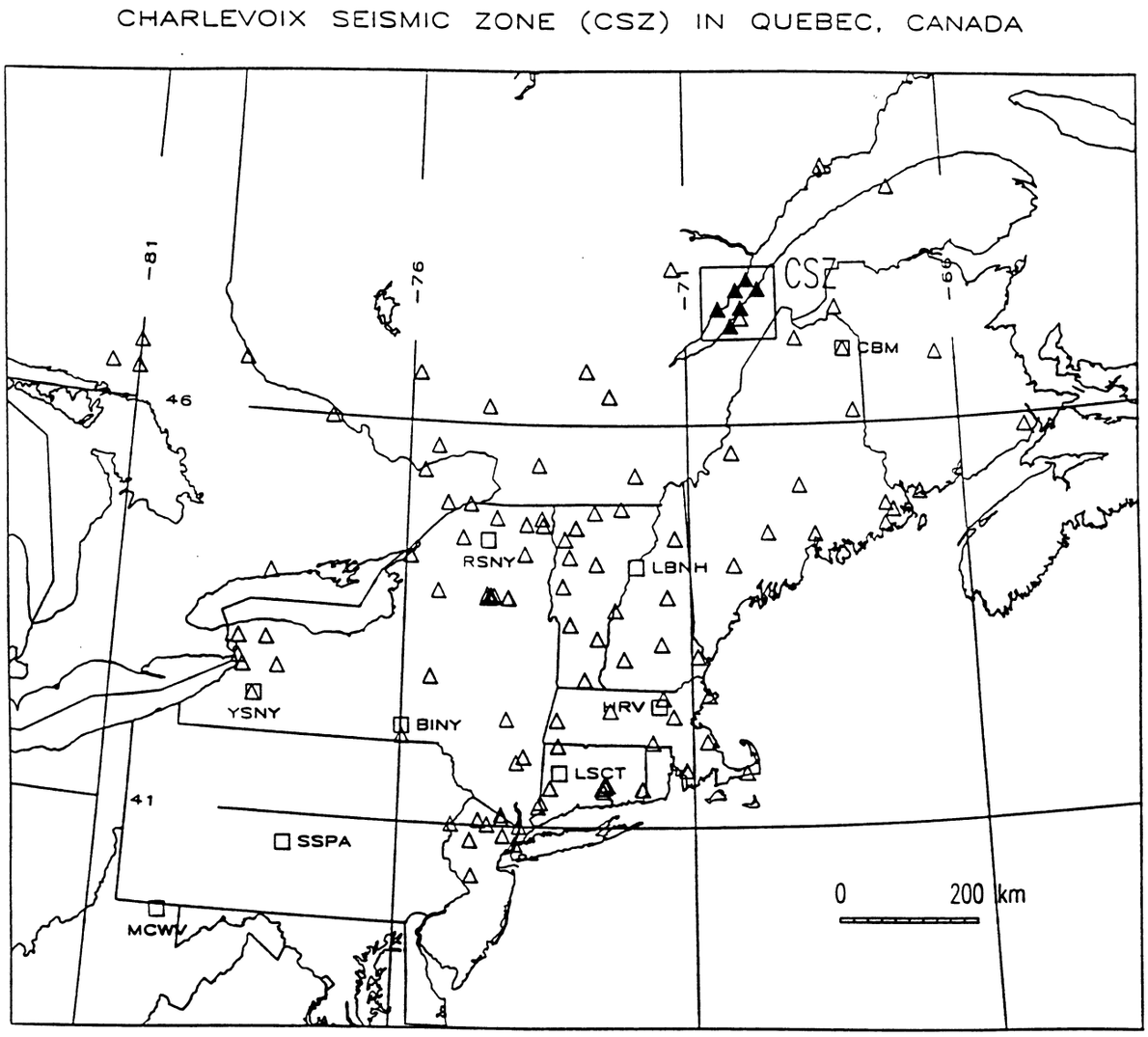

Figure 1: Map of northeastern North America with a box bounding the Charlevoix Seismic Zone (CSZ) of Quebec, Canada. Included are the regional seismic stations (open triangles) of the ECTN (Eastern Canada Telemetered Network), CLTN (Charlevoix Telemetered Network) shown as the filled triangles within the CSZ, NESN (New England Seismic Network), and the Lamont-Doherty Network in New York, New Jersey, and northwestern Vermont. Also shown are the new USNSN (United States National Seismic Network) stations (small boxes with station names) of the USGS. Three-component data recorded by the CLTN was analyzed to obtain precise relative locations of the seismicity in the CSZ.

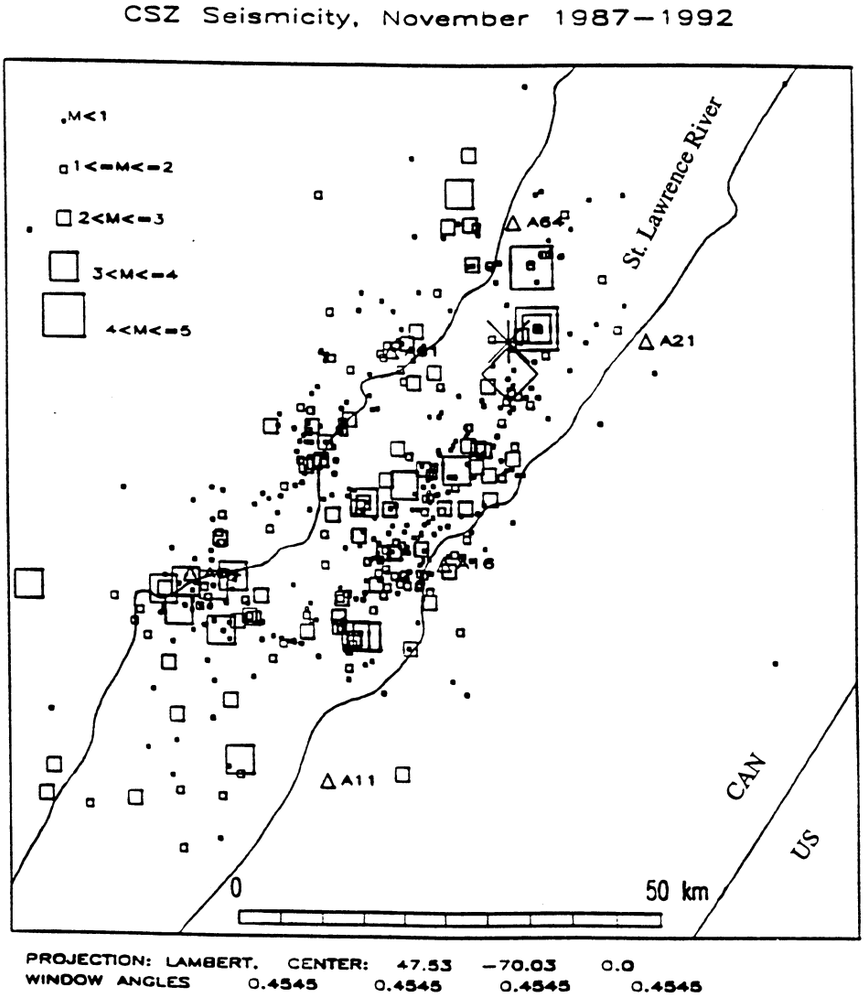

Figure 2: Seismicity (squares) of the Charlevoix Seismic Zone (CSZ) in Quebec, Canada for November 1987-1992. The 1925 (m_b=6.5) and the 1979 (m_b=5.0) earthquakes are shown as an asterisk and a diamond, respectively. The triangles mark the locations of the CLTN stations.

on scale at local distances, thus providing well recorded digital waveforms for a substantial number of events. The quality and amount of waveform data available for the CSZ make this region attractive for the application of the waveform correlation and relative event location techniques.

METHOD

Waveform correlation and relative locations for earthquakes

A precise location for hypocenters of earthquakes within a seismic zone is fundamental for characterizing the seismicity. However, the absolute location of earthquakes depends on not only precise readings of arrival times for seismic phases, but also on the velocity model used in fitting the data. Errors in this model and in arrival time readings will introduce an error into the absolute locations. Simultaneous inversion for hypocenters and velocity structure using a large set of events is one way of reducing the model-induced errors (*e.g.*, Aki and Lee, 1976; Crosson, 1976; Spencer and Gubbins, 1980; Thurber, 1981). The relative event location technique (*e.g.*, Jordan and Sverdrup, 1981; Poupinet *et al.*, 1984; Ito, 1985; Fremont and Malone, 1987; Thorbjarnadottir and Pechmann, 1987) is another way of addressing the hypocenter accuracy versus velocity uncertainty trade-off. The underlying principle of this approach is that, for a given seismic phase and receiver, the difference between the arrival times from two events close to one another is much less sensitive to the velocity structure than are the absolute arrival times from each individual event. If the separations among events of a cluster are much smaller than the hypocentral distances to the observing station, ray paths from the cluster events to the station will be essentially identical. Therefore, the systematic errors due to an incorrect velocity model will have no effect on the accuracy of the relative event locations.

A cross-correlation analysis technique either in the frequency domain (*e.g.,* Poupinet *et al.*, 1984; Ito, 1985) or in the time domain (Frankel, 1982; Pechmann and Kanamori, 1982) is generally used to quantitatively characterize the degree of similarity of seismic waveforms from a cluster of earthquakes close in space and to measure their differential arrival times of P and S waves in an accurate, objective, and consistent manner. An obvious advantage of using this approach is that it avoids the timing error introduced by different analysts picking P and S arrival times. The time domain analysis (Frankel, 1982; Pechmann and Kanamori, 1982) typically allows us to read the arrival times with an accuracy of one sample interval, while a cross-spectral analysis (Poupinet *et al.*, 1984; Ito, 1985) can get timing precision much better than a sampling interval. Poupinet *et al.* (1984) and Ito (1985) claim that for a waveform with a sampling rate of 100 sps their method has a timing accuracy of about 1 ms, resulting in a location accuracy of 10 m. Their approach involves calculating cross-spectra to obtain coherency and phase spectra. The delay time t (i.e., differential time) of the two time series is obtained by fitting a straight line through the phase spectrum with zero intercept. The slope of the straight line is equated to $2\pi ft$, where f is the frequency.

Figure 3 shows an example of the cross-correlation analysis using digital waveforms from the Charlevoix Telemetered Network (CLTN). Vertical component P wave seismograms from a doublet (M1.6 and M4.3) recorded at station A61 in the Charlevoix Seismic Zone (CSZ) show the similarity of the waveforms, even though the amplitudes for the two events differ by a factor of about 500 (Figure 3a, top). The sampling rate of the data is 80 sps. Traditional time domain analysis will give a timing accuracy of only about 0.0125 s (Figure 3a, bottom) and a corresponding location accuracy of about 100 m, which is not sufficient for highly precise relative locations. We applied the cross-spectral analysis to the P waveforms shown in the top frame of Figure 3a and calculated the differential arrival time for the P wave window to be about 0.021 s (Figure 3b). The timing resolution is about 1 ms. However, the spectral-analysis involves time-consuming calculations and fitting the line to the phase spectrum, which is not feasible for processing a large volume of data.

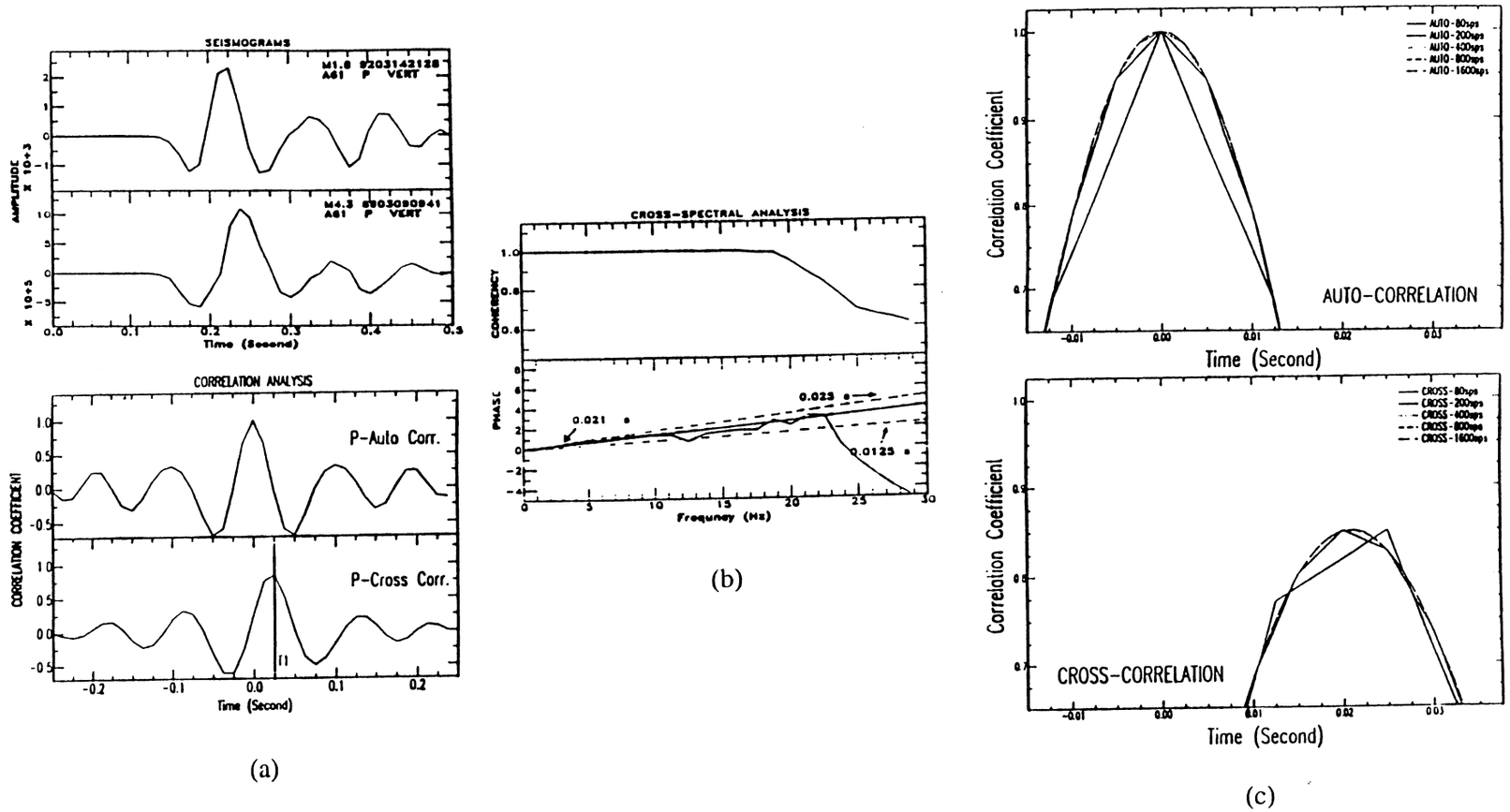

Figure 3: a) Two P waveforms (top), their auto- and cross-correlations (bottom). b) The coherency and phase spectra of the cross-spectrum of the P waveforms in (a). The slope (.021 s) best fitted to the phase component indicates the minimum resolvable sampling interval by the relationship $2\pi ft$. c) The technique of oversampling data in the time domain to more accurately measure the peak cross-correlation amplitude representing the time difference between the onset of the P waves shown in (a). Oversampling yields a best estimate of the P wave differential time of about .021 s. This is comparable to the result from the cross-spectral analysis in (b).

In order to improve the calculation efficiency, we developed a simpler and faster analysis method in the time domain, which has a timing accuracy similar to the cross-spectral method (Poupinet *et al.*, 1984; Ito, 1985) and a quadratic curve interpolating method in the time domain (Deichmann and Garcia-Fernandez, 1992). We oversampled the P wave time series of the master and slave events with an interpolating FIR (Finite Impulse Response) filter (Tapley and Tull, 1991). Figure 3c shows the auto- and cross-correlation functions for different sampling rates. The maximum peak of the auto-correlation functions is always at 0 seconds and the function shapes remain symmetric. The cross-correlation function curves show asymmetry for the lower sampling rates (80 and 200 sps), but become symmetric for higher sampling rates (> 400 sps). The maximum peaks of the cross-correlation functions are at 0.025 s and 0.020 s for sampling rates 80 and 200 sps, respectively. Above 400 sps the peaks converge at 0.021 s, which is consistent with the result of the cross-spectral method (Figure 3b).

The ability of the relative event location method to calculate high precision locations of earthquakes is founded on waveform and hypocenter similarity of the events. Figure 4a shows the waveforms of three events recorded at two stations with different azimuths. The P and S waveforms of the three events for each station are quite similar and have almost identical differential arrival times, as indicated by no moveout of the S phase when they are aligned to the initial P phase. The nearly identical relative locations of the three earthquakes are displayed in Figure 4b. In contrast, the waveforms of three other earthquakes in Figure 5a have less similarity at two stations with different azimuths and display a noticeable moveout of the S phases with the P phases aligned. The relative locations of these three earthquakes are separated by about 1 to 2 km (Figure 5b).

RESULTS AND CONCLUSIONS

We have applied the waveform correlation and relative event location method to CLTN waveform data to relocate hypocenters of earthquakes in the CSZ, assuming a one-layer crustal model for the CSZ having an average P wave velocity of 6.2 km/s and a Vp/Vs ratio of 1.73 (Anglin and Buchbinder, 1981; Anglin, 1984). The simplified velocity model may slightly bias absolute locations for master events, if strong heterogeneity exists in the medium, but has less effect on the relative locations of a cluster of events. The measurement accuracy of differential arrival times for P and S waves is about 1 ms, resulting in a spatial resolution of about 10 m for the hypocenter locations. The original absolute locations were computed by the Geophysics Division of the Geological Survey of Canada using a modified version of the HYPO program and the velocity model mentioned above (Drysdale *et al.*, 1991).

The hypocenters of 214 digitally recorded earthquakes occurring in the CSZ between 1987 and 1993 were relocated. 3-D spatial transformations (rotation of a volume of hypocenters defined by a rectangular coordinate system) of the earthquake locations were performed using the 3-D geometry viewer module of AVS (Application Visualization Systems, Advanced Visual Systems, Inc., 1992). The original HYPO and relative event locations of these earthquakes are shown in Figures 6 and 7, respectively. In map view (Figures 6a and 7a), the seismicity is divided into two major groups separated by a gap in the St. Lawrence River. The first group, bounded by the box in Figures 6a and 7a, is located mainly along or near the northwest shore of the St. Lawrence River, while the second larger group is located to the southeast in the river. The spatial distributions of both groups show a general northeast trend parallel to the river. The group in the box in Figures 6a and 7a shows a significant change in spatial distribution after relocation, forming two apparent lineations striking northeast with a gap between them (Figure 7a). This group is discussed in more detail in the next section about correlation of the seismicity with mapped faults. In map view, the relocated seismicity of the group in the river (Figure 7a) exhibits somewhat closer clustering of the epicenters than the original HYPO locations of the same group (Figure 6a), but no major lineations are readily observed. The closer clustering in Figure 7a produces a few apparent

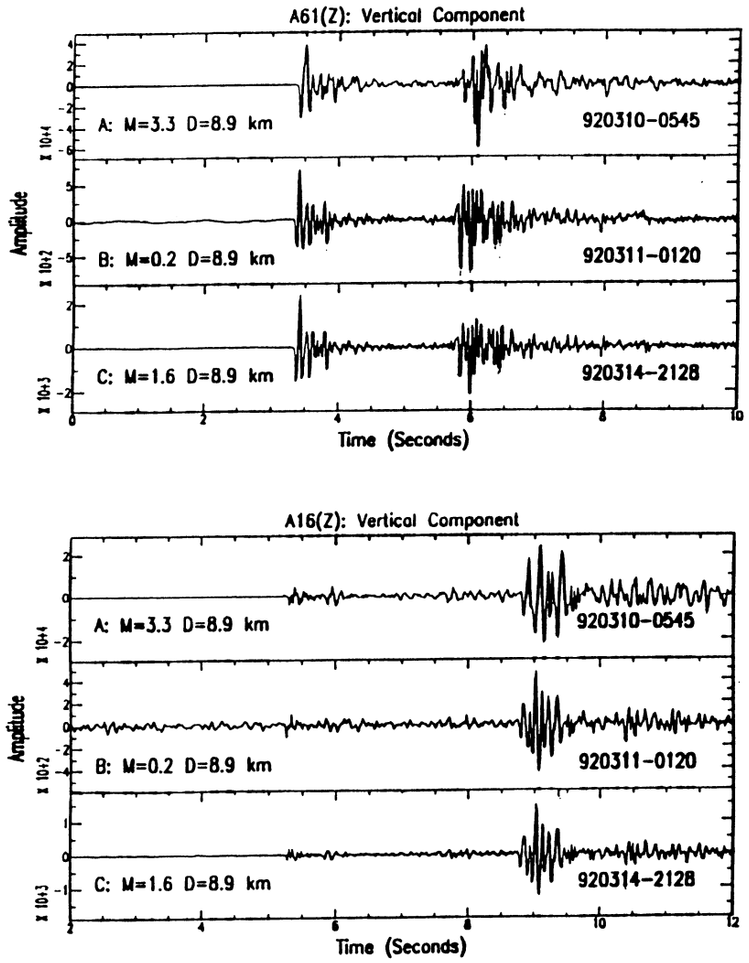

(a)

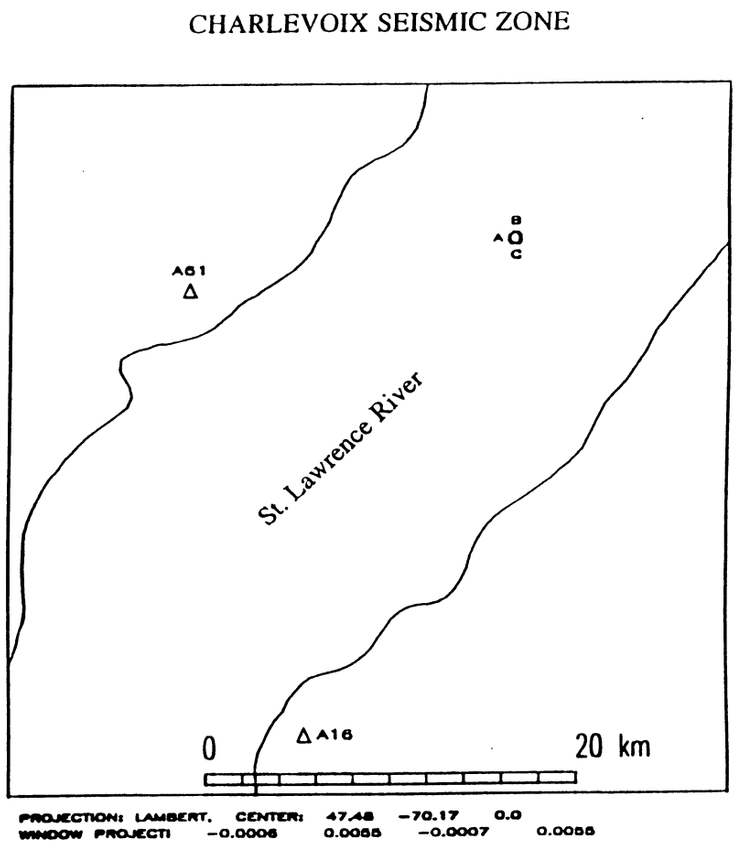

(b)

Figure 4: a) Vertical component seismograms of three earthquakes having essentially the same hypocenter. The waveforms are very similar, and with the P waves aligned, no moveout of the S wave is observed at two stations at different azimuths from the earthquake cluster. b) Relative locations of the three earthquakes (A, B, and C).

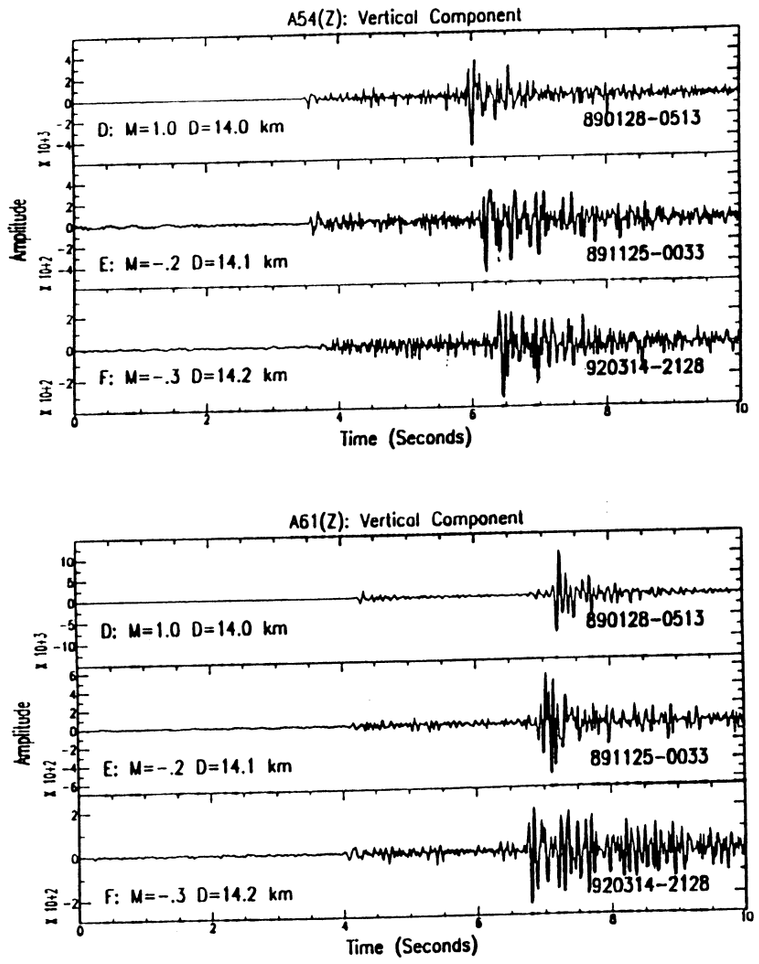

(a)

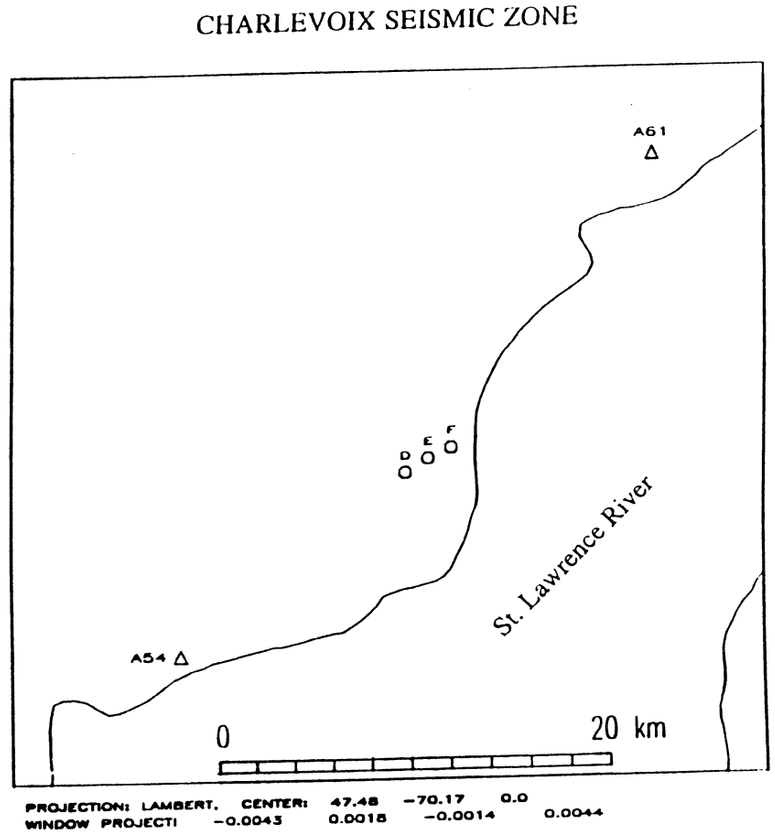

(b)

Figure 5: a) Vertical component seismograms of three earthquakes having different hypocenters. The waveforms show less similarity than those for the cluster having almost identical hypocenters in Figure 4. With P aligned, the S waves display a distinct moveout. b) The relative locations of the three earthquakes (D, E, and F) indicate an epicentral separation of 1-2 km.

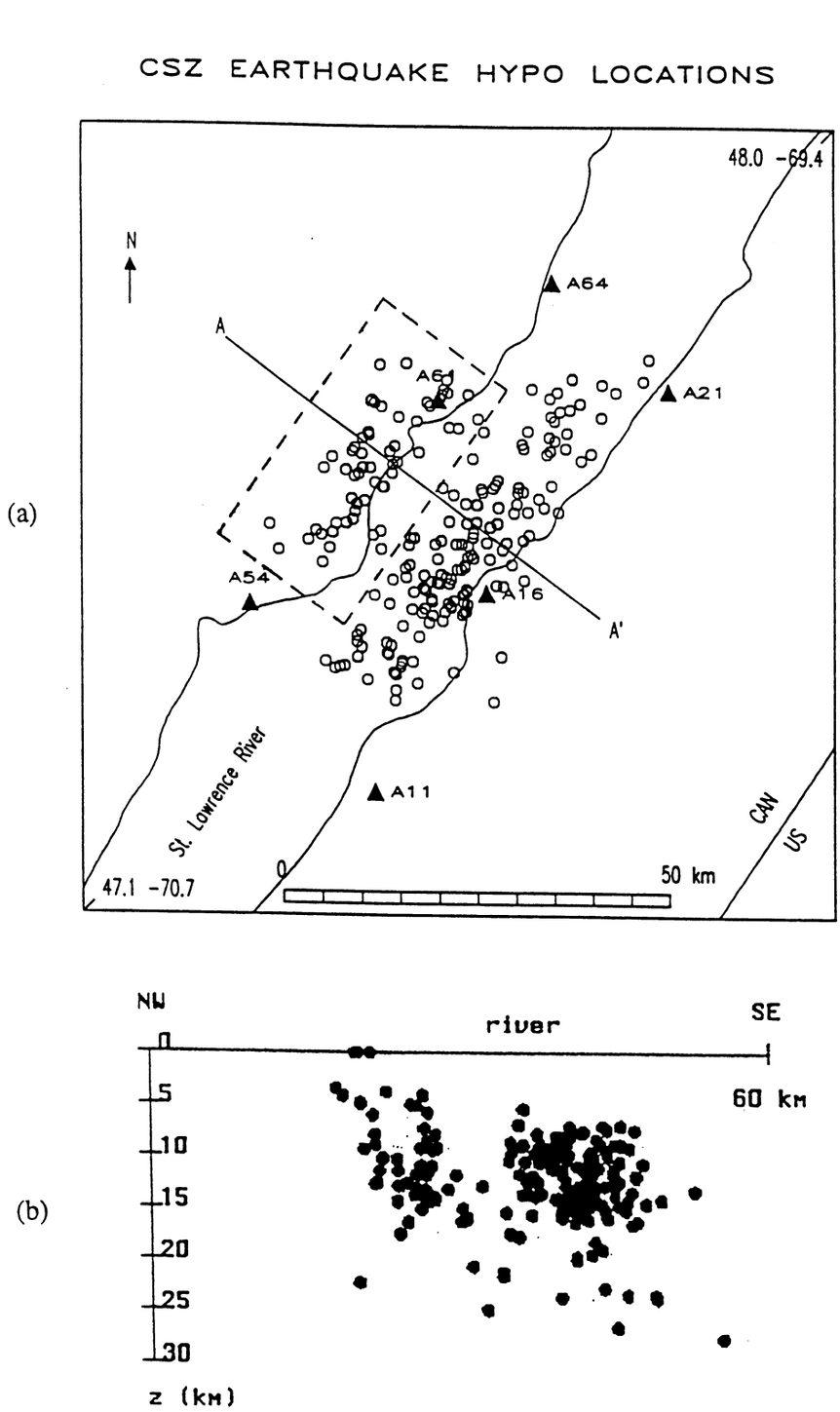

Figure 6: HYPO locations of all the earthquakes used in this study shown in a) Map view, and b) Vertical cross-section. Line AA' in Figure 6a marks the location of the cross-section. The view perpendicular to the plane of the cross-section is along a strike N36°E.

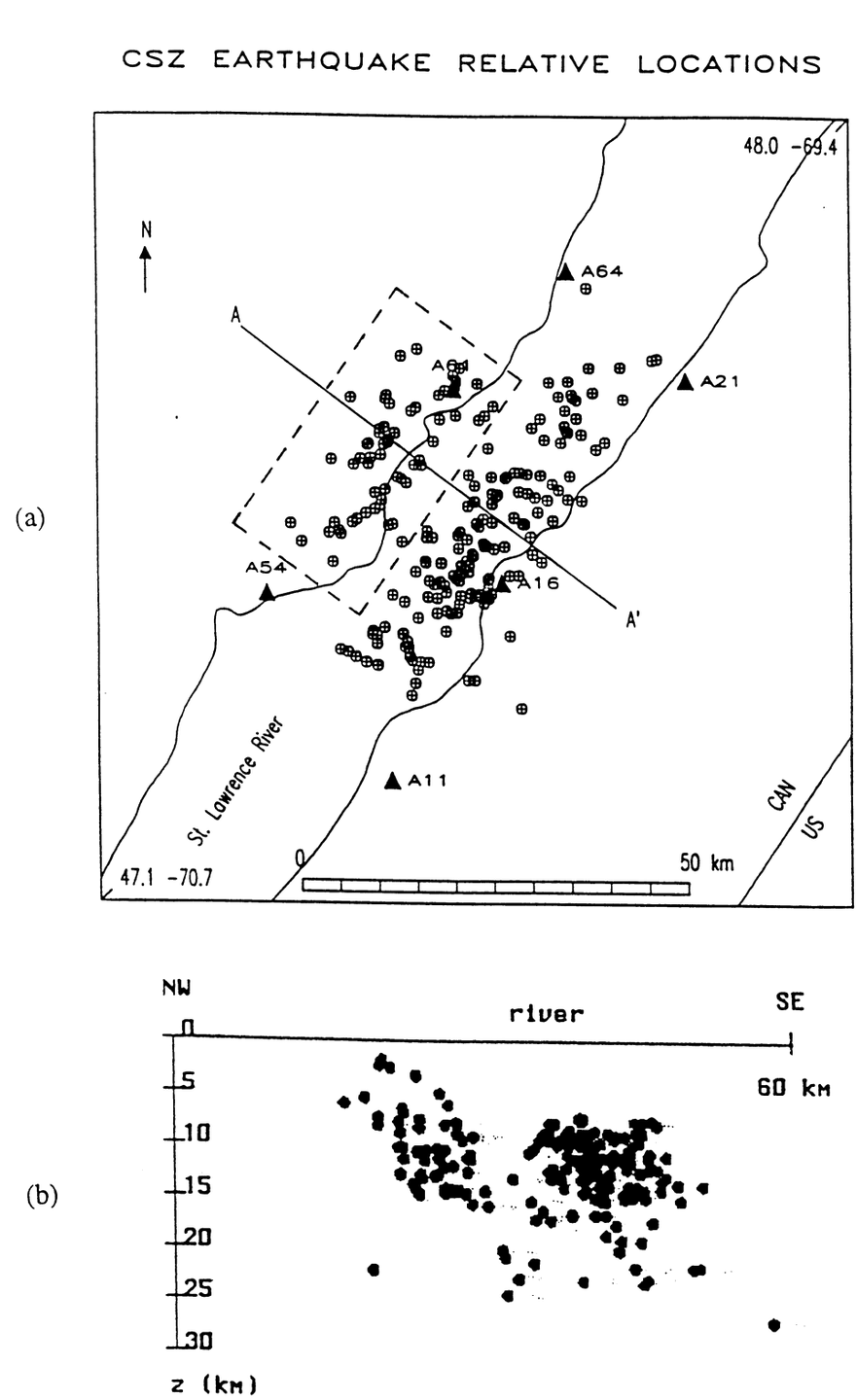

Figure 7: Relative event locations of all the earthquakes used in this study shown in a) Map view, and b) Vertical cross-section. Line AA' in Figure 7a marks the location of the cross-section. The view perpendicular to the plane of the cross-section is along a strike N36°E.

short linear patterns of seismicity with different orientations, which may imply a complex fracture system of small active faults in the river.

In cross-section (Figures 6b and 7b) the seismicity clearly defines a V-shaped seismic zone in the St. Lawrence River both for the HYPO and relative event locations. The viewing direction perpendicular to the cross-section in Figures 6 and 7 is N36°E. This agrees with the result of earlier investigations by Anglin *et al.* (1984) and Buchbinder *et al.* (1988), in which they identified the V-shaped feature along a similar strike. After relocation, the V-shape appears to be more sharply resolved. In particular, a few hypocenters on the northwest side have shifted from the surface to the basement rock beneath a major aseismic contact with overlying sedimentary deposits dipping gently to the southeast (Buchbinder *et al.*, 1988). In Figure 8, the cross-sections of Figures 6b and 7b have been rotated about a horizontal axis parallel to the plane of the cross-sections. This spatial transformation produces a view along the same strike (N36°E), but now with a plunge of about 21° to the northeast. At this orientation some of the deep hypocenters to the northeast in the CSZ become aligned with the shallower seismicity defining the sides of the V in Figures 6b and 7b. The view in Figure 8 seems to delineate more accurately the actual extent of the V-shaped seismic zone, particularly with the relative locations (Figure 8b).

Correlation of Seismicity with Geology

Our work to date has produced good correlation with the geology in specific subregions of the CSZ. Figure 9 shows the spatial correlation of the earthquakes (bounded by the box in Figures 6a and 7a) with mapped faults along the northwest shore of the St. Lawrence River, using the original HYPO locations (Figure 9a) and the relative event locations (Figure 9b) computed in this study. Two northeast trending lineations of epicenters become apparent after relocation and demonstrate a strong spatial association with some north to northeast striking faults. This is best illustrated by the correspondence of the epicenters of one lineation with the fault running directly along the northwest shore of the river. The second lineation, further to the northwest, is grouped mainly in two clusters elongated toward the northeast and aligned with one another along a strike parallel to the first lineation. The two clusters of this second lineation terminate near the ends of two mapped faults and may define these faults as discontinuous features. However, the cluster to the southwest shows a strong northeasterly alignment with the cluster to the northeast (around station A61) and some intervening epicenters. This alignment may indicate that the mapped fault underlying the northeast cluster extends as a subsurface feature to the southwest, possibly emerging again as the northeast trending fault mapped just to the northwest of station A54.

Several relocated events show no close spatial correlation with the two northeast trending lineations of epicenters or the mapped faults associated with them. In general, these events either are not located near the mapped faults or correlate better with one of the faults striking southeast. Figures 10 and 11 present the HYPO and relative event locations, respectively, of the same set of earthquakes shown in Figure 9, except with these "outliers" removed. The cross-sections in Figures 10 and 11 are viewed along an axis striking N50°E. In depth view after relocation (Figure 11b), the two northeast trending lineations appear to be almost vertically dipping planer features. In a study of the geology of the Charlevoix region Rondot (1979) reported that the mapped faults striking northeast near the northwest shore of the St. Lawrence River are Precambrian normal faults. Other faults similar in orientation to these exposed ones cut through the basement rocks underlying the river to the southeast. Both groups of faults are inferred to be rifting structures related to the opening of the Atlantic Ocean 600-700 and 150-200 MYA (Hasegawa, 1986), which are now reactivated by the present stress regime (Hasegawa, 1986; Buchbinder *et al.*, 1988; Adams *et al.*, 1988). The high angle dip of the two seismic features in Figure 11b is consistent with the fault geometry of a rift structure. As a point of interest, these two planer distributions of hypocenters, which may delineate active faults, are best resolved at a strike of N50°E. In a shear-wave splitting study of earthquakes located along the northwest shore of the St. Lawrence River in

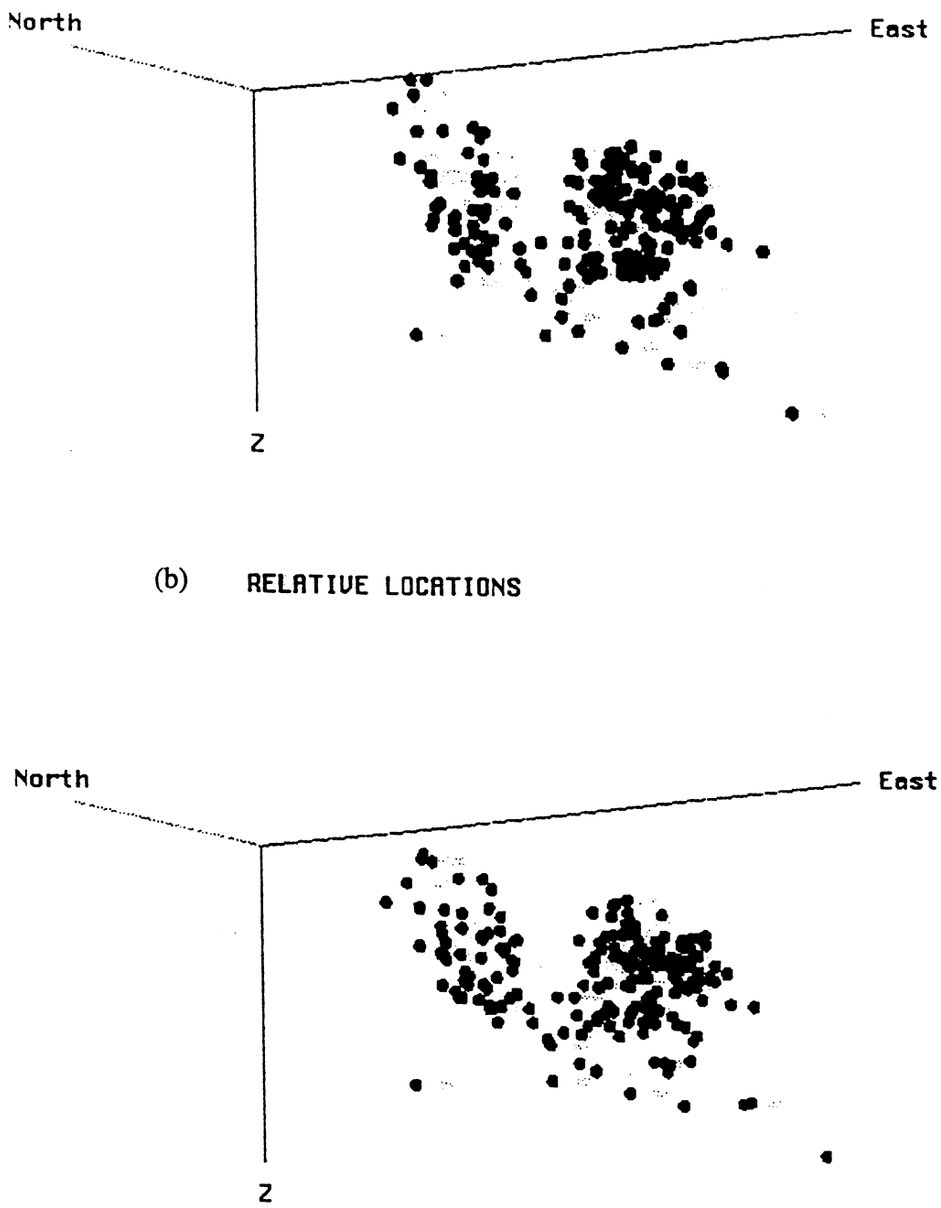

Figure 8: Oblique cross-sections of a) the HYPO locations, and b) the relative event locations of all the earthquakes used in this study. The view perpendicular to the plane of the cross-section is along an axis striking N36°E and plunging 21° to the northeast.

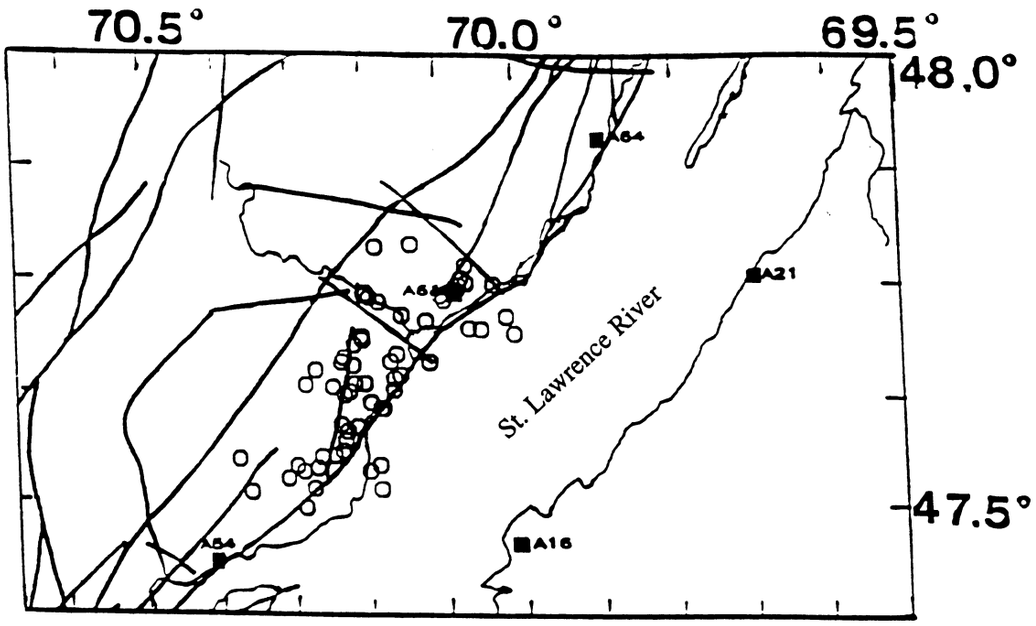

(a)

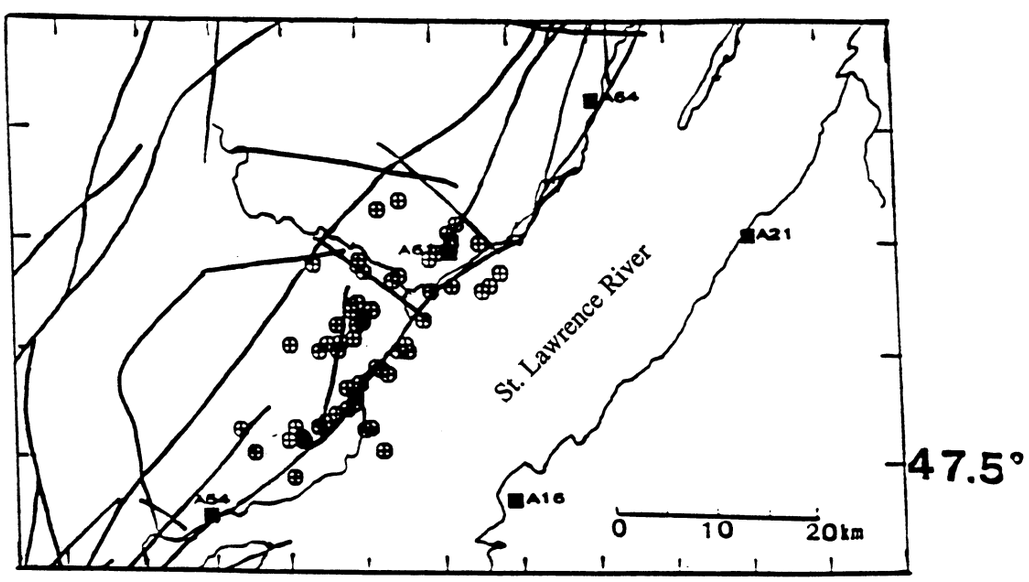

(b)

Figure 9: a) HYPO locations (open octagons), and b) Relative event locations (crossed octagons) of earthquakes (the group bounded by the box in Figures 6a and 7a) superposed on a fault map (Rondot, 1979) of the CSZ. After relocation of the earthquakes, two linear trends of epicenters are more clearly defined striking about parallel to the St. Lawrence River and some of the major mapped faults. In particular, the linear trend along the shore of the river shows a strong spatial correlation with an extensive fault striking northeast. The spatial correlation of a few of the epicenters with a southeast trending cross fault, southwest of Station A61, is improved after event relocation.

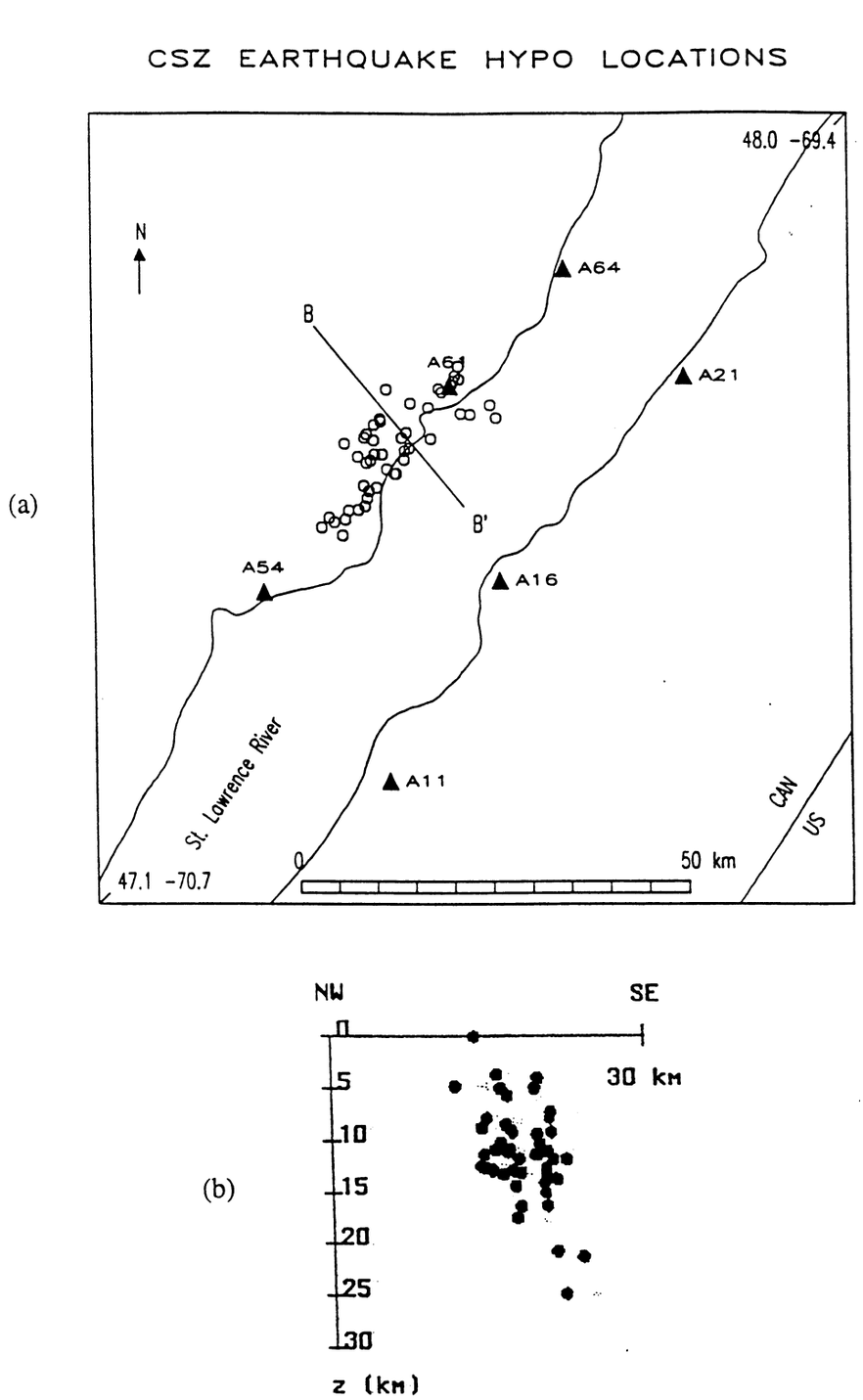

Figure 10: a) Map view, and b) Vertical cross-section of the HYPO locations of the earthquakes in Figure 9a with "outliers" removed. Line BB' in Figure 10a marks the location of the cross-section.

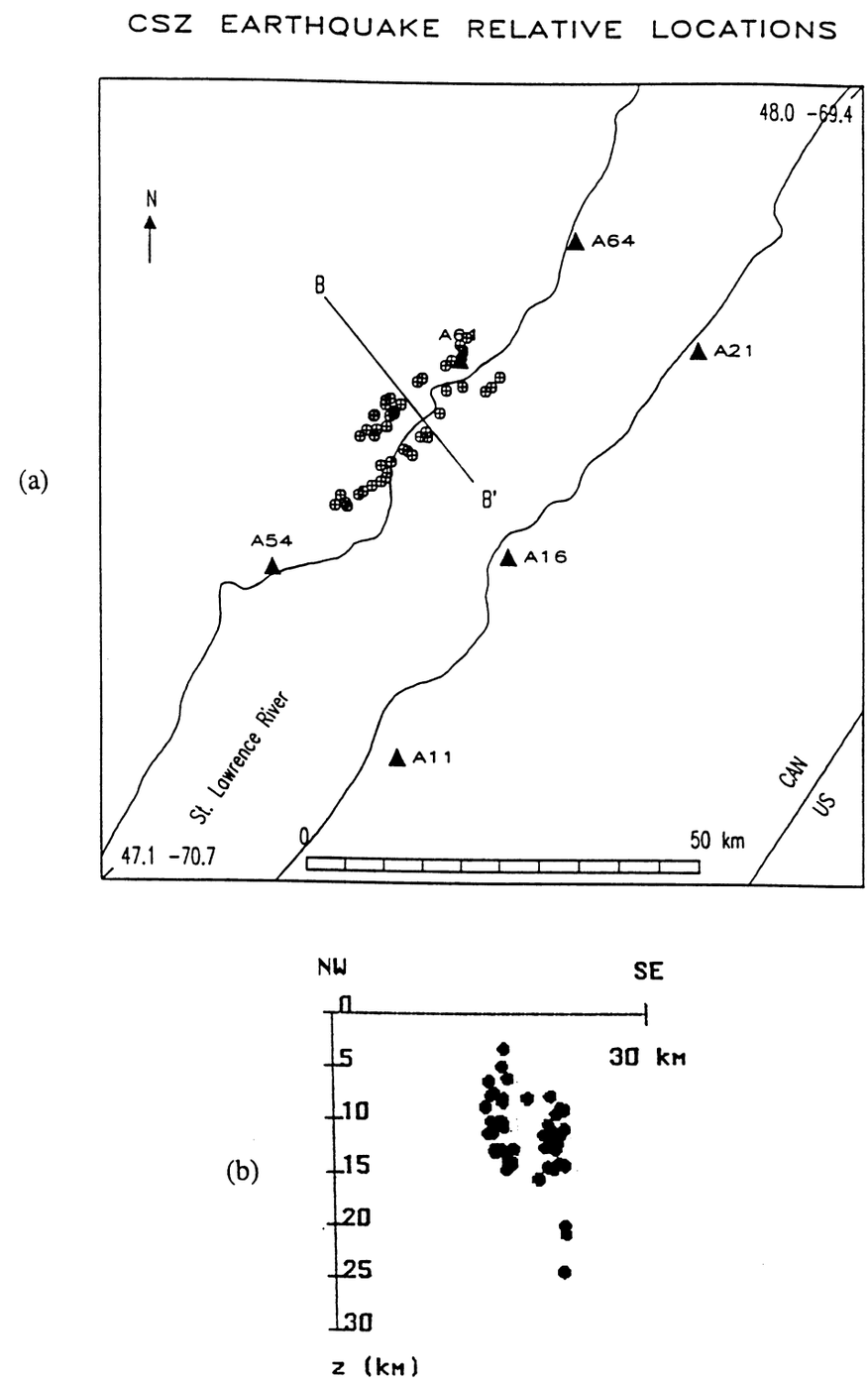

Figure 11: a) Map view, and b) Vertical cross-section of the relative event locations of the earthquakes in Figure 9b with "outliers" removed. Line BB' in Figure 11a marks the location of the cross-section. The hypocenter distribution shows two well defined planer features, each with a vertical dip. These two planer features are not well resolved in the HYPO locations in Figure 10b.

the CSZ, Doll *et al.* (1994) found an average S polarization angle of N48°E for 32 events having approximately northeast polarization directions. The S polarization angle has been interpreted as the azimuth of near-vertical cracks in the basement rock beneath the CSZ (Buchbinder *et al.*, 1985, 1989; Doll *et al.*, 1994). The relative event location and shear-wave splitting results are consistent and suggest that the orientation of the faults inferred from the hypocenter distributions in Figure 11b is well constrained.

Cross-sections of the seismicity subparallel to the St. Lawrence River have revealed some planer seismic features striking approximately northwest across the river. Figures 12 and 13 show HYPO and relative event locations, respectively, for a subgroup of earthquakes extending across the St. Lawrence River in the southwest part of the CSZ. Two planer features, both striking approximately northwest, appear to be defined by the distribution of hypocenters in the cross-sections in Figures 12b and 13b. One is vertical and is intersected by a second feature dipping to the northeast. Both the HYPO and relative event locations show these features well. Studies of the shear-wave splitting of earthquakes in the CSZ (Buchbinder *et al.*, 1985, 1989; Doll *et al.*, 1994) have revealed a dominant northeast orientation of S polarization angles assumed to be produced by near vertical cracks striking in that direction. However, the polarization angles of some earthquakes in these studies, including a few in the region of the events shown in Figures 12 and 13, have orientations more consistent with the northwest strikes of the inferred seismic features in these two figures. The spatial pattern of hypocenters and shear-wave splitting evidence may indicate the existence of active cross faults intersecting the northeast striking faults beneath and to the northwest of the St. Lawrence River (Figure 9).

Two northeast trending mapped faults in Figure 9, one along the north shore of the St. Lawrence River and another about 15 to 20 km to the northwest of the first, are long, continuous features extending the entire length of the CSZ. Similarly, large scale faults are inferred to strike northeast in the basement rock beneath the St. Lawrence River (Hasegawa, 1986; Buchbinder *et al.*, 1988). On the northwest side of the river, these structures are intersected by other faults striking approximately northwest in Figure 9. Cross faults, possibly extending across the river to the southeast, might act as barriers to rupture propagation, thus limiting the maximum size of a northeast trending seismogenic feature to a dimension much less than the total length (~ 80 km) of the CSZ. If faulting can only occur along shorter fault segments, the size of the largest earthquake possible in the CSZ might be significantly less than estimates derived using the overall dimensions of the zone.

REFERENCES

Adams, J., J. Sharp, and M. Stagg, 1988. New Focal mechanisms for southeastern Canada earthquakes, Geological Survey of Canada, *Open File 1892,* 109 pp.

Advanced Visual Systems, Inc., 1992. Application Visualization Systems, Software Release 4.

Aki, K., and W. H. K. Lee, 1976. Determination of three-dimensional velocity anomalies under a seismic array using first P arrival times from local earthquakes. Part I. A homogeneous initial model, *J. Geophys Res., 81,* 4781-4399.

Anglin, F. M., and G. Buchbinder, 1981. Microseismicity in the mid-St. Lawrence Valley Charlevoix zone, Quebec, *Bull. Seism. Soc. Am., 71,* 1553-1560.

Anglin, F. M., 1984. Seismicity and faulting in the Charlevoix zone of the St. Lawrence Valley, *Bull. Seism. Soc. Am., 74,* 596-603.

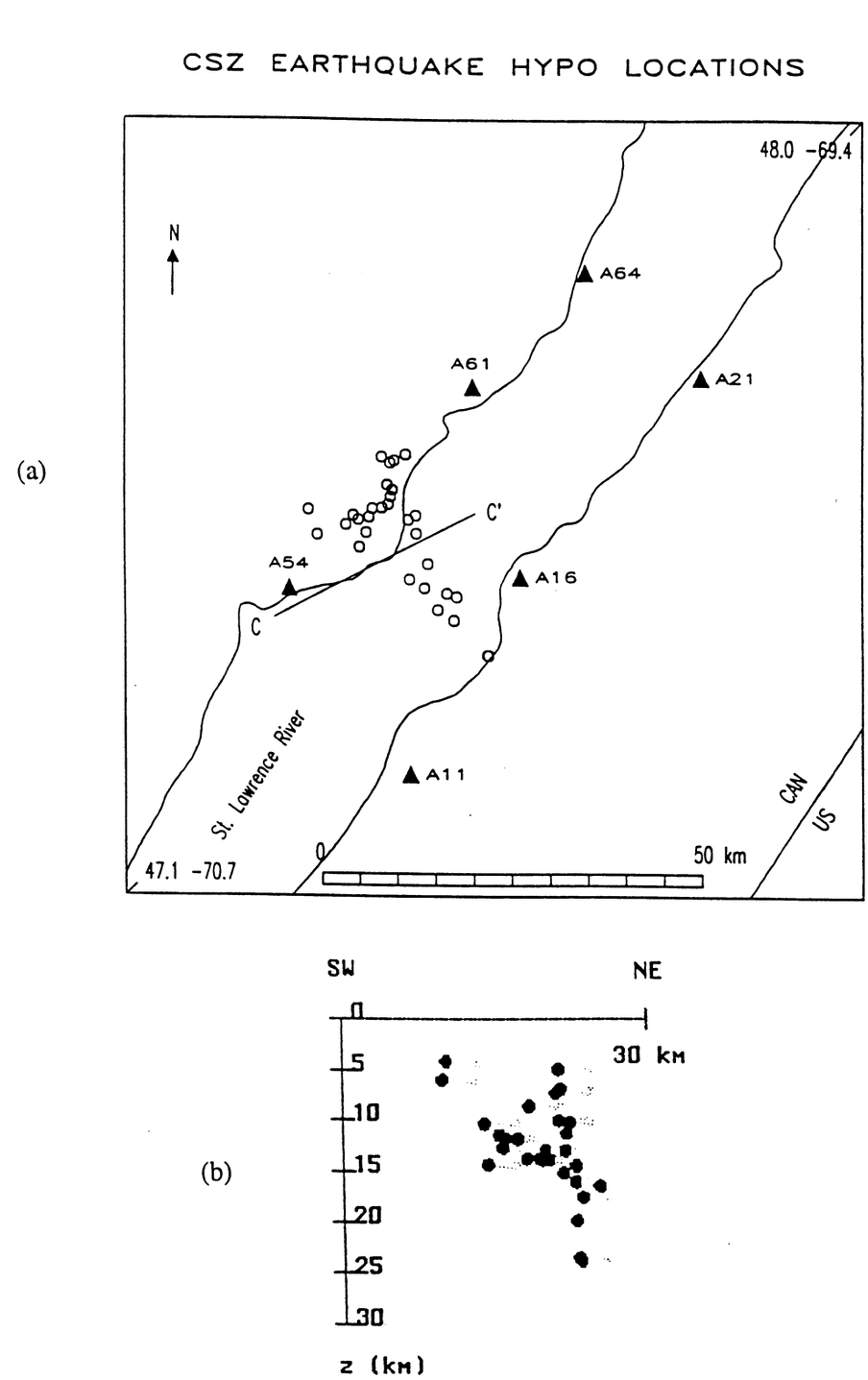

Figure 12: a) Map view, and b) Vertical cross-section of the HYPO locations for a subgroup of earthquakes in the southwestern part of the CSZ. Line CC' in Figure 12a marks the location of the cross-section. The hypocenter distribution appears to define two planer features, one vertical and a second intersecting the first at an oblique angle. Features like these may represent active cross faults cutting across the system of long northeast trending faults in the CSZ.

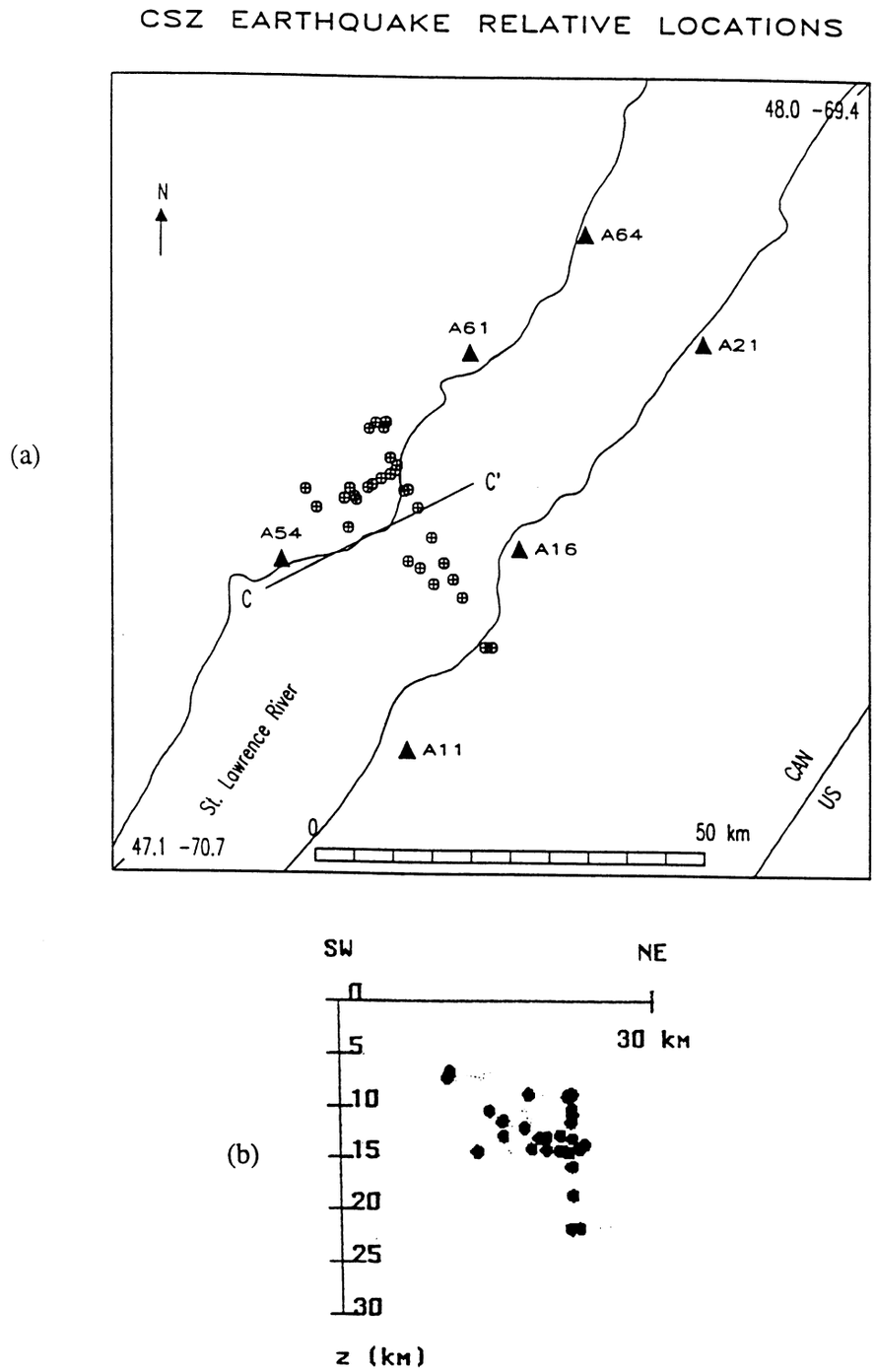

Figure 13: a) Map view, and b) Vertical cross-section of the relative event locations for the same subgroup of earthquakes shown in Figure 12. Line CC' in Figure 13a marks the location of the cross-section. The planer features in Figure 12b are also observed here, but with tighter clustering of the hypocenters.

Bent, A. L., 1992. A re-examination of the 1925 Charlexoix, Quebec earthquake, *Bull. Seism. Soc. Am., 82,* 2097-2113.

Buchbinder, G.G.R., 1985. Shear-wave splitting and anisotropy in the Charlevoix Seismic Zone, Quebec, *Geophys. Res. Lett., 12,* 425-428.

Buchbinder, G.G.R., 1989. Azimuthal variations in P-wave travel times and shear-wave splitting in the Charlevoix seismic zone, *Tectonophysics, 165,* 293-302.

Buchbinder, G.G.R., A. Lambert, R.D. Kurtz, D. R. Bower, F.M. Anglin, and J. Peters, 1988. Twelve years of geophysical research in the Charlevoix seismic zone, *Tectonophysics, 156,* 193-224.

Crosson, R.S., 1976. Crustal structure modeling of earthquake data. Part 1. Simultaneous least squares estimation of hypocenter and velocity parameters, *J. Geophys Res., 81,* 3036-3046.

Deichmann, N., and M. Carcia-Fernandez, 1992. Rupture geometry form high-precise relative hypocenter locations of microearthquake clusters, *Geophys. J. Int., 110,* 501-517.

Doll, Jr., C., Y. Li, M.N. Toksöz, 1994. Spatial variation in shear-wave splitting in the Charlevoix Seismic Zone of Quebec and its relationship to the local and regional stress fields, *EOS, Trans., AGU, Spring Meeting Supplement, 75,* no. 16, 235.

Drysdale, J.A., R.B. Horner, C.L. Spindler and M. Lamontagne, 1991. Canadian Earthquakes National Summary January - March 1991, Geological Survey of Canada, Ottawa, Canada.

Ebel, J.E., P.G. Somerville and J.D. McIver, 1986. A study of the source parameters of some large earthquakes of northeastern North America, *J. Geophys Res., 91,* 8231-8247.

Frankel, A., 1982. Precursors to a magnitude 4.8 earthquake in the Virgin Islands: spatial clustering of small earthquakes, anomalous focal mechanisms and earthquake doublets, *Bull. Seism. Soc. Am., 72,* 1277-1294.

Fremont, M., and S. Malone, 1987. High precision relative locations of earthquakes at Mount St. Helens, Washington, *J. Geophys. Res., 92,* 10223-10233.

Hasegawa, H.S., 1986. Seismotectonics in eastern Canada: An overview with emphasis on the Charlevoix and Miramichi regions. *Earthquake Notes, 57,* 83-94.

Hasegawa, H.S. and R.J. Wetmiller, 1980. The Charlevoix earthquake of 19 August 1979 and its seismo-tectonic environment, *Earthquake Notes, 51,* 23-37.

Ito, A., 1985. High-resolution relative hypocenters of similar earthquakes by cross-spectral analysis method, *J. Phys. Earth, 33,* 279-294.

Jordan, T.H. and K.A. Sverdrup, 1981. Teleseismic location techniques and their application to earthquake clusters in the South-Central Pacific, *Bull. Seism. Soc. Am., 71,* 1105-1130.

Klein, F.W., 1978. Hypocenter Location Program Hypoinverse, *United States Geological Survey Open-file Report 78-694,* Menlo Park, California, 113 pp.

Pechmann, J. C., and H. Kanamori, 1982. Waveforms and spectra of preshocks and aftershocks of the 1979 Imperial Valley, California, earthquake: Evidence of fault heterogeneity? *J. Geophys. Res., 87,* 10579-10597.

Poupinet, G., W.L. Ellsworth and J. Frechet, 1984. Monitoring velocity variations in the crust using earthquake doublets: An application to the Calaveras fault, California, *J. Geophys. Res., 89,* 5719-5731.

Rondot, J., 1979. Reconnaissances geologiques dans Charlevoix-Saguenay. Ministere des Richesses Naturelles, Quebec, DPV-682.

Smith, W.E.T., 1962. Earthquakes of eastern Canada and adjacent areas 1534-1927, *Pub. Dominion Obs., 26,* 271-301.

Spencer, C., and D. Gubbins, 1980. Travel-time inversion for simultaneous earthquake location and velocity determination in laterally varying media, *Geophys. J. R. Astron. Soc., 63,* 95-116.

Stevens, A.E., 1980. Reexamination of some larger La Malbaie, Quebec earthquakes (1924-1978), *Bull. Seism. Soc. Am., 70,* 529-557.

Tapley W.C., and J.E. Tull, 1991. SAC (Seismic Analysis Code), Users manual, Lawrence Livermore National Laboratory, Livermore, California.

Thorbjarnadottir, B.S. and J.C. Pechmann, 1987. Constraint on relative earthquake locations from cross-correlation of waveforms, *Bull. Seism. Soc. Am., 77,* 1626-1634.

Thurber, C.H., 1981. Earth structure and earthquake locations in the Coyote lake area, central California, *Ph. D. Thesis,* Massachusetts Institute of Technology.

Wetmiller, R.J. and J. Adams, 1990. An earthquake doublet in the Charlevoix seismic zone, Quebec, in *Current Research, Part B, Geological Survey of Canada, Paper 90-1,* 105-113.

Li, Y., C. Doll, Jr., W. Rodi, and M.N. Toksöz, 1994. Precise relative location of earthquakes for characterizing seismicity and its geological association in the Charlevoix Seismic Zone, Quebec, *Seism. Res. Lett., 65, SSA Abstract 201*, 60.

Li, Y., C. Doll, Jr., and M.N. Toksöz, 1994. Estimates of source time functions and associated parameters using the EGF method for the M=1.5 to 4.5 earthquakes in the Charlevoix, Miramichi, and New Hampshire seismic zones, *Seism. Res. Lett., 65,* 32.

Li, Y., C. Doll, Jr., and M.N. Toksöz, 1994. Source characterization and fault plane determinations for M_{bLg} 1.2 - 4.4 earthquakes in the Charlevoix Seismic Zone, Quebec, Canada, submitted to *Bull. Seism. Soc. Am.*

CHARACTERIZING SEISMICITY AND ITS GEOLOGICAL ASSOCIATION IN NORTHEASTERN NORTH AMERICA WITH RELATIVE LOCATION AND EMPIRICAL GREEN'S FUNCTIONS

Contract no. 1434-94-G-2421

M. Nafi Toksöz
Massachusetts Institute of Technology
Earth Resources Laboratory
42 Carleton Street
Cambridge, Massachusetts 02142
(617)-253-7852
FAX (617)-253-6385
email: nafi@erl.mit.edu
Program Element II.2

Non-technical Project Summary

The relationship between earthquakes and active faults is not well understood in eastern North America. This research is intended to improve our knowledge of this relationship. Research techniques are being applied to earthquake data recorded in the Charlevoix Seismic Zone (CSZ) of Quebec, Canada to characterize active faults in that region. Earthquake source parameters are determined to estimate the amount and spatial distribution of the energy moving outward from the earthquake source. Measurements of earthquake source parameters and spatial patterns of seismicity determined from high accuracy locations of earthquakes are being combined to attempt to characterize potentially active geologic faults and to estimate maximum earthquake size in the CSZ.